ฤทธิ์ต้านการเพิ่มจำนวนเซลล์มะเร็ง Jurkat ของอนุภาคทองคำนาโนที่เชื่อมต่อกับเพปไทด์ SAHM1

นางสาวมุกธิดา ทิพยมณฑา

วิทยานิพนธ์นี้เป็นส่วนหนึ่งของการศึกษาตามหลักสูตรปริญญาวิทยาศาสตรมหาบัณฑิต
สาขาวิชาเทคโนโลยีชีวภาพ
คณะวิทยาศาสตร์ จุฬาลงกรณ์มหาวิทยาลัย
ปีการศึกษา 2560

ANTIPROLIFERATIVE ACTIVITY AGAINST JURKAT CELLS OF SAHM1 PEPTIDE CONJUGATED GOLD NANOPARTICLES

Miss Mukthida Thippayamonta

A Thesis Submitted in Partial Fulfillment of the Requirements
for the Degree of Master of Science Program in Biotechnology
Faculty of Science
Chulalongkorn University
Academic Year 2017

Thesis Title	ANTIPROLIFERATIVE ACTIVITY AGAINST JURKAT CELLS OF SAHM1 PEPTIDE CONJUGATED GOLD NANOPARTICLES
By	Miss Mukthida Thippayamonta
Field of Study	Biotechnology
Thesis Advisor	Associate Professor Kittinan Komolpis, Ph.D.
Thesis Co-Advisor	Associate Professor Tanapat Palaga, Ph.D.
	Assistant Professor Stephan T.dubas, Ph.D.

Accepted by the Faculty of Science, Chulalongkorn University in Partial Fulfillment of the Requirements for the Master's Degree

.....Dean of the Faculty of Science
(Professor Polkit Sangvanich, Ph.D.)

THESIS COMMITTEE

.....Chairman
(Associate Professor Nattaya Ngamrojanavanich, Ph.D.)

.....Thesis Advisor
(Associate Professor Kittinan Komolpis, Ph.D.)

.....Thesis Co-Advisor
(Associate Professor Tanapat Palaga, Ph.D.)

.....Thesis Co-Advisor
(Assistant Professor Stephan T.dubas, Ph.D.)

.....Examiner
(Associate Professor Chanpen Chanchao, Ph.D.)

.....External Examiner
(Associate Professor Primchanien Moongkarndi, Ph.D.)

มุกธิดา ทิพยมณฑา : ฤทธิ์ต้านการเพิ่มจำนวนเซลล์มะเร็ง Jurkat ของอนุภาคทองคำนาโนที่เชื่อมต่อกับเพปไทด์ SAHM1 (ANTIPROLIFERATIVE ACTIVITY AGAINST JURKAT CELLS OF SAHM1 PEPTIDE CONJUGATED GOLD NANOPARTICLES) อ.ที่ปรึกษาวิทยานิพนธ์หลัก: รศ. ดร.กิตตินันท์ โกมลภิส, อ.ที่ปรึกษาวิทยานิพนธ์ร่วม: รศ. ดร.ธนาภัทร ปาลกะ, ผศ. ดร.สเตฟาน ที ดูบาส, 63 หน้า.

ในปัจจุบันการรักษาโรคมะเร็งประกอบด้วย การผ่าตัด การฉายรังสี และการรักษาด้วยเคมีบำบัด ถึงแม้ว่าผู้ป่วยจะได้รับการรักษาตามวิธีข้างต้นจนหายเป็นปกติ แต่ก็มีจำนวนไม่น้อยที่ได้รับผลข้างเคียงจากการรักษา ดังนั้นงานวิจัยจำนวนมากจึงสนใจที่จะศึกษาหาทางเลือกใหม่ในการรักษาโรคมะเร็ง ซึ่งแนวทางการรักษาที่เป็นที่สนใจมากที่สุดคือการใช้ตัวยาที่ถูกออกแบบให้มีฤทธิ์ฆ่าเซลล์มะเร็งอย่างจำเพาะเจาะจงต่อเป้าหมาย และไม่เป็นอันตรายต่อเซลล์ปกติใกล้เคียง Stapled α-helical peptide derived from mastermind-like I หรือ SAHM1 ก็เป็นหนึ่งในเพปไทด์ที่ถูกออกแบบขึ้นและมีการรายงานถึงฤทธิ์ที่จำเพาะต่อการยับยั้งการเพิ่มจำนวนของเซลล์มะเร็ง อย่างไรก็ตามฤทธิ์ดังกล่าวของเพปไทด์ยังมีข้อจำกัดในเรื่องของความสามารถเข้าสู่เซลล์ของเพปไทด์เพื่อไปยังเป้าหมายที่จะออกฤทธิ์ จึงเป็นที่มาของงานวิจัยนี้เพื่อศึกษาการใช้อนุภาคทองคำระดับนาโนเป็นตัวนำส่งเพปไทด์ SAHM1 เข้าสู่เซลล์ Jurkat โดยเริ่มจากการสังเคราะห์อนุภาคทองคำระดับนาโนผ่านการเกิดปฏิกิริยาระหว่าง $HAuCl_4$ กับ trisodium citrate ที่ความเข้มข้นต่างๆ เพื่อให้ได้มาซึ่งอนุภาคทองคำที่มีขนาดเส้นผ่านศูนย์กลาง 20 40 และ 60 นาโนเมตร จากนั้นเชื่อมติดเพปไทด์เข้ากับอนุภาคทองคำระดับนาโนโดยอาศัย thiolated polyethylene glycol (PEG) เป็นตัวเชื่อม ในการทดสอบความเป็นพิษต่อเซลล์ Jurkat โดยวิธี MTT assay พบว่าอนุภาคทองคำระดับนาโน SAHM1 และ thiolated PEG ที่เชื่อมติดกับอนุภาคทองคำระดับนาโนทำให้การมีชีวิตของเซลล์ลดลงอยู่ที่ระดับประมาณ 70 เปอร์เซ็นต์ ในขณะที่ SAHM1 ที่ความเข้มข้น 62.5 และ 125 ไมโครโมลาร์ ที่เชื่อมติดกับอนุภาคทองคำขนาด 20 นาโนเมตร มีความเป็นพิษต่อเซลล์อย่างเด่นชัดที่สุด เมื่อเทียบกับเซลล์กลุ่มควบคุม และเซลล์กลุ่มทดลองอื่นๆ ดังนั้นจึงสรุปได้ว่าอนุภาคทองคำขนาด 20 นาโนเมตร มีส่วนช่วยเพิ่มฤทธิ์ในการยับยั้งการเพิ่มจำนวนเซลล์ Jurkat ของ SAHM1 ที่ความเข้มข้น 62.5 และ 125 ไมโครโมลาร์ ได้ นอกจากนี้ในการศึกษาลักษณะการตายของเซลล์ Jurkat โดยการย้อมสีเซลล์ด้วย Annexin V และ propidium iodide พบว่าเซลล์ที่ได้รับ SAHM1 ที่เชื่อมติดกับอนุภาคทองคำขนาด 20 นาโนเมตร เป็นเวลา 24 และ 48 ชั่วโมง เซลล์ที่ตายจะเกิดการตายในขั้น early apoptosis และ late apoptosis

สาขาวิชา เทคโนโลยีชีวภาพ ลายมือชื่อนิสิต .....

ปีการศึกษา 2560 ลายมือชื่อ อ.ที่ปรึกษาหลัก .....

ลายมือชื่อ อ.ที่ปรึกษาร่วม .....

ลายมือชื่อ อ.ที่ปรึกษาร่วม .....

5872025723 : MAJOR BIOTECHNOLOGY
KEYWORDS: APOPTOSIS; GOLD NANOPARTICLE; JURKAT CELL; SAHM1; TOXICITY

MUKTHIDA THIPPAYAMONTA: ANTIPROLIFERATIVE ACTIVITY AGAINST JURKAT CELLS OF SAHM1 PEPTIDE CONJUGATED GOLD NANOPARTICLES. ADVISOR: ASSOC. PROF. KITTINAN KOMOLPIS, Ph.D., CO-ADVISOR: ASSOC. PROF. TANAPAT PALAGA, Ph.D., ASST. PROF. STEPHAN T.DUBAS, Ph.D., 63 pp.

In general, treatments of cancer may involve medication, surgery, radiation and chemotherapy. Although these treatments are successful at a certain satisfactory level, their side effects are not acceptable for some patients. Thus, many researches have been investigated alternative methods to cure cancer. A technique of interest is the use of targeted drug therapy in which drug is designed to selectively kill only the cancer cells and to do no harm on the normal cells. Stapled α-helical peptide derived from mastermind-like I or SAHM1 is a small peptide which has been reported to have antiproliferative activity against cancer cells. However, its use is limited by degradation during cell penetration and transport inside the cell. In this study, gold nanoparticles (GNPs) were studies as the carrier of SAHM1 in penetrating into Jurkat cells in order to enhance antiproliferative activity of SAHM1. GNPs were synthesized by reaction between trisodium citrate and $HAuCl_4$ at different conditions to obtain the particles with the averaged size of 20 nm, 40 nm and 60nm. SAHM1 was attached to the GNPs using thiolated polyethylene glycol (PEG) as the linker. Cytotoxicity of GNPs, thiolated PEG, thiolated PEG-GNPs, SAHM1 and SAHM1-(thiolated PEG)-GNPs was investigated by conventional MTT assay. Cell viabilities of Jurkat cells decreased to about 70% when separately treated with GNPs, SAHM1 and thiolated PEG-GNPs as compared to those of the untreated cells. Cell viabilities of the cell treated with SAHM1-GNPs noticeably decreased only when 20 nm GNPs coated with 62.5 µM and 125 µM SAHM1 were used as compared to those of cells treated with GNPs, thiolated PEG, thiolated PEG-GNPs and SAHM1. Therefore, enhancement of antiproliferative activity of SAHM1 was found when 20 nm GNPs coated with 62.5 µM and 125 µM SAHM1 were used. Study of mode of program cell death by staining cells with Annexin V and propidium iodide after cell treatment with SAHM1-GNPs for 24 h and 48 h revealed that most cells died in early apoptosis and late apoptosis.

Field of Study: Biotechnology
Academic Year: 2017

Student's Signature .....
Advisor's Signature .....
Co-Advisor's Signature .....
Co-Advisor's Signature .....

ACKNOWLEDGEMENTS

This thesis would not have been possible without the support of many people. I would like to thank all those who have helped and encouraged me during my study. First and foremost I am sincerely thankful to my advisor, Assoc. Prof. Kittinan Komolpis for providing me the inspiration and guidance throughout this research. Great thanks go to my co-advisor, Assoc. Prof. Tanapat Palaga and Asst. Prof. Stephan Dubas for their immense support, suggestion and invaluable help.

Deepest gratitude is also due to all thesis committee, Assoc. Prof. Nattaya Ngamrojanavanich, Assoc. Prof. Chanpen Chanchao, and Assoc.Prof. Primchanien Moongkarndi, external committee from Department of Microbiology, Faculty of Pharmacy, Mahidol University, for their comments and suggestions which greatly assisted to improve my thesis in all aspects.

I would like to thank Mrs. Songchan Puthong, Mr. Anumart Buakeaw and Miss Umaporn Pimpitak for their support and sharing their invaluable experience.

I would also like to thank the Institute of Biotechnology and Genetic Engineering (IBGE), Chulalongkorn University, for facilities and support.

My deepest gratitude goes to my family for their unflagging love and supporting without condition.

CONTENTS

Page

Page

Page

LIST OF TABLE

LIST OF FIGURE

LIST OF ABBREVIATION

ANOVA	Analysis of variance
CO_2	Carbon dioxide
CSL	Named after the vertebrate, Drosophila and *C. elegans* homologs, CBF1, Su(H), and LAG-1
DDI	Double deionized water
FITC	Fluorescein isothiocyanate
GNPs	Gold nanoparticles
GSIs	Gamma (γ)-secretase inhibitors
h	hour
ICN	Intracellular subunits
mg	Milligram
min	Minute
mL	Millilitre
mm	Millimeter
mM	Millimolar
Mn	Molecular weight
mV	Millivolt
NaCl	Sodium chloride
nm	Nanometer
NOTCH	Neurogenic locus notch homolog protein
OD	Optical density
PBS	Phosphate buffered saline

PI	Propidium I odide
rpm	Revolutions per minute
S.D.	*Standard deviation*
UV-Vis	UltaViolet-Visible
v/v	Volume by volume
^{o}C	Degree Celsius
λ_{max}	Maximum absorbance wavelength
µM	Micromolar
µL	Microlitre
%	Percent

CHAPTER I

INTRODUCTION

Cancer is the leading cause of death worldwide. Over the years, chemotherapy is commonly used in current practice to treat cancer via intravenous administration but also to elicit toxicity to normal cells, leading to severe side effects in patients. Several approaches are available to enhance the activity and diminish the side effect of chemotherapeutics treatment. One approach is the use of drug delivery system that targets only at cancer cells.

Many researches in recent years have reported, small peptides with pro-apoptotic activity can be regarded as promising anticancer agents if a delivery system improves their efficacy (Akrami et al., 2016). Stapled α-helical peptides derived from mastermind-like1 (SAHM1) is one of therapeutic compounds that has been reported to have anticancer activity (Moellering et al., 2009). SAHM1 affects NOTCH1 target gene levels and the global expression profile of the NOTCH signaling program in human and murine T-cell acute lymphocytic leukemia (T-ALL). Acute lymphocytic leukemia (ALL) is a cancer that starts at the early form of white blood cells called lymphocytes in the bone marrow. Leukemia cells usually invade the blood very quickly. They can spread to other parts of the body, including the lymph nodes, liver, spleen, central nervous system, and testicles. The term “acute” means that the leukemia can progress quickly, and if not treated, would probably be fatal within a few months. Lymphocytic means that it is developed from early (immature) forms of lymphocytes, a type of white blood cell. Any type of early blood-forming cell of the bone marrow can turn into a leukemia cell. Once this change happens, the leukemia

cells will not mature normally. The leukemia cells could reproduce quickly, and might not die when they should. Instead they survive and build up in the bone marrow. Over time, these cells spill into the bloodstream and spread to other organs, where they can keep other cells from functioning normally.

In order to kill the cancer cells, the peptide must penetrate thru the membrane to be inside the cell. However, the peptide could be destroyed during the penetration. Therefore, anticancer peptide (ACP) must be stabilized so that it can reach the target cancer sites. Stapling of the peptide and use of gold nanoparticle (GNP) has been studied to enhance pharmacologic performance and stability of the peptide and to overcome cell protection. Gold nanoparticle conjugates express unique properties such as increasing binding affinity and selectively targeting the specific tissue or cell when delivered systemically.

It has been reported that conjugation of GNP and ACP could be used to enhance the anticancer potency. An effective system for ROS scavenging activity which induces the apoptosis in Retinoblastoma cancer cells was observed as a result of the synergistic effect of the GNPs-Pep-A (Kalmodia et al., 2016). In another study, GNP was used successfully as the carrier of prostate-tumor-specific bombesin peptide to deliver optimal payload of the peptide at the cancer receptor sites (Chanda et al., 2010).

In this study, gold nanoparticle (GNP) will be synthesized and then conjugated with SAHM1. Cytotoxicity, antiproliferative and apoptosis inducing activity of the obtained conjugate was studied in the Jurkat leukemic T-cell line. Information obtained in this research could be used to improve the effectiveness of an emerging concept in cancer treatment and would create a new drug delivery system.

CHAPTER II

LITERATURE REVIEWS

2.1 Gold nanoparticles (GNPs)

2.1.1 History of gold nanoparticles

Nanotechnology has been employed and developed for over a thousand years. One of the most examples known in history is medieval stained glass artisans. They embed gold nanoparticles in the 'glass matrix' in order to generate the wine red color in the windows. The size of the gold nanoparticles defines the variations in color. Another example is the Lycurgus Cup made by the Romans at around the 4th-century (AD). In daylight, it appears green and when light is transmitted through the glass, its color changes to red. The change in color of this cup is due to the glass embedding tiny amounts of gold nanoparticle in its surface (Figure 2.1). In recent years, gold nanoparticle has been used for the development of more efficient technology due to its applications such as biotechnology, vehicles for drug delivery, and electronic storage systems (Mody et al., 2010).

Figure 2. 1 Medieval stained glass artisans (A) and the Lycurgus Cup (B)
(Source: https://en.wikipedia.org/wiki/Medieval_stained_glass)

2.1.2 Biomedical applications of gold nanoparticle

Among the multiple branches of nanotechnology applications, one of the major applications is in biomedicine. As nanoparticle has size similar to many biological molecules, it shows different physical properties compared to bulk materials. Gold nanoparticles (GNPs) are relatively inert in biological environment, and suitable for several biomedical applications. For example, gold nanoparticles have been successfully employed in radiotherapy for cancer, computed tomography imaging and as drug carriers (X. Zhang, 2015). Moreover, GNPs have been shown to enhance the antiproliferation and apoptosis of human hepatoma cells induced by Paclitaxel, a chemotherapeutic drug (Cai et al., 2008; Wei et al., 2007). Size of GNPs is smaller than that of human cells about a thousand times with theirs small size, GNPs can conjugate with biomolecules or drugs so that the conjugates can go to the target and interact on the surface or inside the target cells. These may revolutionize cancer treatment and diagnosis (Qian et al., 2013).

However, using GNPs as drug delivery and other biomedical applications need to specifically, safely and effectively direct to a specific tissue or disease site. GNP-base drug delivery has not been achieved in targeting in vivo, due to the overall size of the conjugate typically more than 50 nm in diameter which prohibits efficient extravasation (Cai et al., 2008)

2.1.3 Size and shapes

GNPs are stable metal nanoparticle and their unique physical and optical properties are shown in Table 2.1 These properties of GNP depend on particle size, and shape that can be prepared in numerous shapes such as nanospheres, nanorods, and

nanoshells as illustrated in Figure 2.2 (Jain et al., 2006) . Meanwhile, many researches that study the use of GNP as drug delivery pay attention in using GNP in shape of nanosphere. As in the research of Rock et al., 2008, they proposed doxorubicin (DOX) loaded oligonucleotides (ONTs) attached to GNPs in shape of nanosphere as a drug delivery system for cancer chemotherapy. And they suggested that these would promising drug delivery systems for cancer therapy(Rock and Kono, 2008).

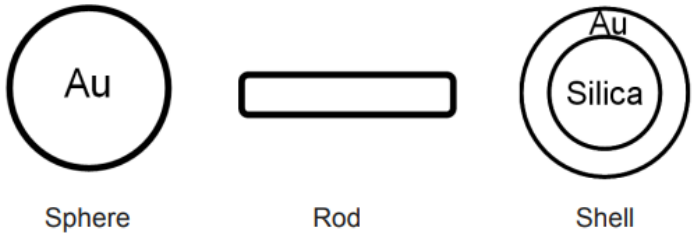

Figure 2. 2 Different types of gold nanoparticles
(Cai et al., 2008)

Gold nanospheres known as gold colloids which have the size of 2 nm to over 100 nm can be synthesized by varying the citrate and $HAuCl_4$ solution as reported in 1951(Turkevich et al., 1951). Generally, the larger the amount of the citrate solution, the smaller the size of gold nanospheres. In addition, there are many researches that used gold nanoparticle in nanosphere shape to study in the field of biomedical. The research reported that the size and shape is important in relation to cellular uptake in vivo (Kim et al., 2009). Moreover, spherical shaped nanoparticles had an increased uptake over rod shaped particles (Chithrani et al., 2006). Another factor is the surface functionality, the peptide or drug should able to penetrate the cell membrane and be internalized. For example, the study of gold nanoparticles capped with the cell penetrating peptides (CPPs) on nuclear location signal (NLS) by using TEM. The conjugates were transported from the extracellular through cell membrane into the

cytoplasm (Nativo *et al.*, 2008). In addition, CCPs-gold nanoparticle conjugates could enter the cytoplasm via endocytosis or directly through the cell membrane. These results showed their functionality in drug delivery systems.

Table 2. 1 Summary of optical and physical properties of spherical standard gold nanoparticles.

Diameter (nm)	Peak SPR Wavelength (nm)	Size Dispersity (+/-nm)	Surface Area (nm2)	Surface/ Volume Ratio	Particle Mass (g)	Molar Mass (g/mol)
5	515-520	<15%	7.85E+01	1.200	1.27E-18	7.64E+05
10	515-520	<15%	3.14E+02	0.600	1.02E-17	6.11E+06
15	520	<12%	7.07E+02	0.400	3.43E-17	2.06E+07
20	524	<12%	1.26E+03	0.300	8.12E-17	4.89E+07
30	526	<12%	2.83E+03	0.200	2.74E-16	1.65E+08
40	530	<12%	5.03E+03	0.150	6.50E-16	3.91E+08
50	535	<10%	7.85E+03	0.120	1.27E-15	7.64E+08
60	540	<10%	1.13E+04	0.100	2.19E-15	1.32E+09
70	548	<10%	1.54E+04	0.086	3.48E-15	2.10E+09
80	553	<10%	2.01E+04	0.075	5.20E-15	3.13E+09
90	564	<8%	2.54E+04	0.067	7.40E-15	4.46E+09
100	572	<8%	3.14E+04	0.060	1.02E-14	6.11E+09

www.cytodiagnostics.com

2.1.4 Advantages of gold nanoparticle

GNPs have many advantages and widely used as a cancer or tumor therapies (Guo et al., 2014). Because GNP has unique physical, optical, and chemical properties, it can deliver cancer drug into cancer cell. (Jain et al., 2006; X. Zhang, 2015). GNPs are biocompatible and available for conjugation with small biomolecules such as DNA, peptide, antibody, proteins, enzymes, and organic dyes as shown in Figure 2.3 (Cai et al., 2008). In addition, GNPs have high surface area which show drug loading capacity (Chithrani et al., 2006). Due to small size and dispersion, GNPs can easily reach to the targeted site by blood circulation system (Kojima et al., 2010) and they are considered to be non-toxic agents because overall cytotoxicity of GNPs is in acceptable level (Khan et al., 2014).

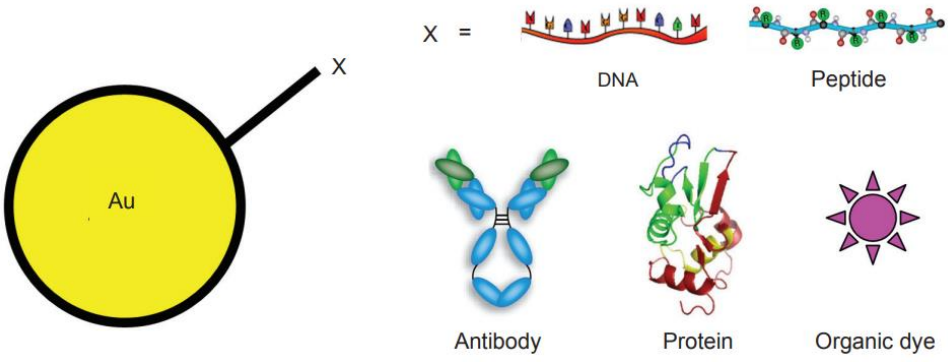

Figure 2. 3 Modification of gold nanoparticles with various molecules for in vitro assays
(Cai et al., 2008)

2.2 Synthesis of gold nanoparticles

GNPs are synthesized by reduction of tetrachloroauric acid ($HAuCl_4$) using different reducing agents which commonly used is citrate under varying conditions.

The particles of colloidal gold would nearly monodisperse gold nanospheres (Turkevich et al., 1951). Furthermore, the particle size of the colloidal gold solution is determined by the number of nuclei around gold nanoparticle surface as shown in Figure 2.4. Thus, the more the nuclei, the smaller the gold particles would be produced. In addition, the amount of the citrate ions is related to the number of nuclei. Therefore, less sodium citrate should be added for producing the larger gold nanoparticles in term of varying sizes is necessary (Wongtangprasert, 2012).

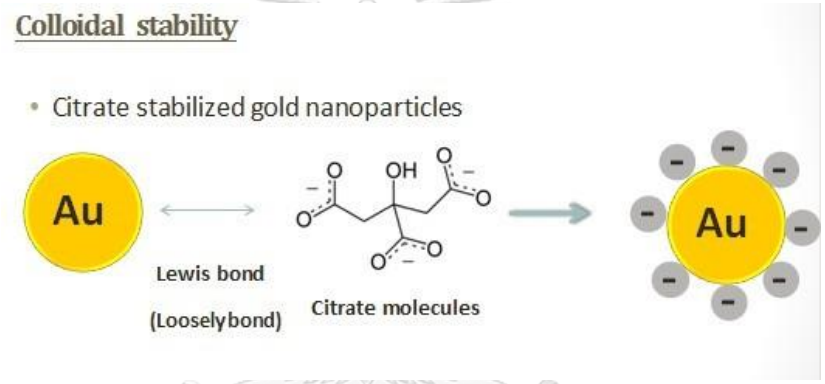

Figure 2. 4 Formation of gold nanoparticle by the citrate capping. (https://yuchinhuang.wordpress.com/author/yuchinhuang/)

GNPs display a single maximum wavelength in the visible range between 510 nm and 550 nm. As shown in Figure 2.5, with increasing particle size, the maximum wavelength would shifts to a longer wavelength while the width of the absorption spectra is related to the size distribution range (Cai et al., 2008).

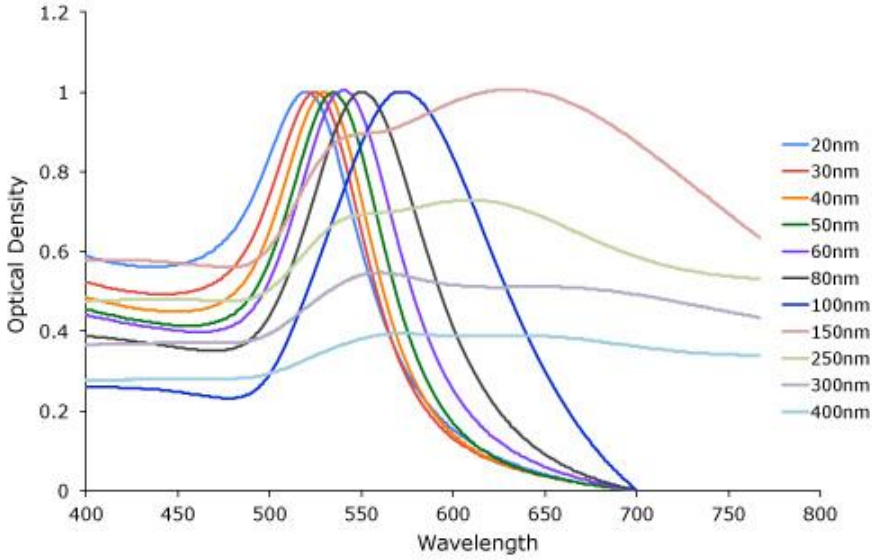

Figure 2. 5 Scanning spectrum of gold nanoparticle in different sizes

www.cytodiagnostics.com

2.3 Tools for characterization of gold nanoparticles

2.3.1 Transmission electron microscopy (TEM)

Transmission Electron Microscopy (TEM) is a vital characterization tool for directly imaging nanomaterials to obtain quantitative measures of particle size, size distribution, and morphology (Rice et al., 2013). TEM uses electromagnets to focus a beam of electrons, which is then transmitted through a particle. Denser parts of the particle absorb more electrons, which makes them look darker on the image. TEM are good because they have a higher resolution than optical microscopes so give a more detailed image. They have a maximum resolution of about 0.0002 µm or about one thousand times higher than optical microscopes and have the maximum useful magnification about x 500,000 (Figure 2.6).

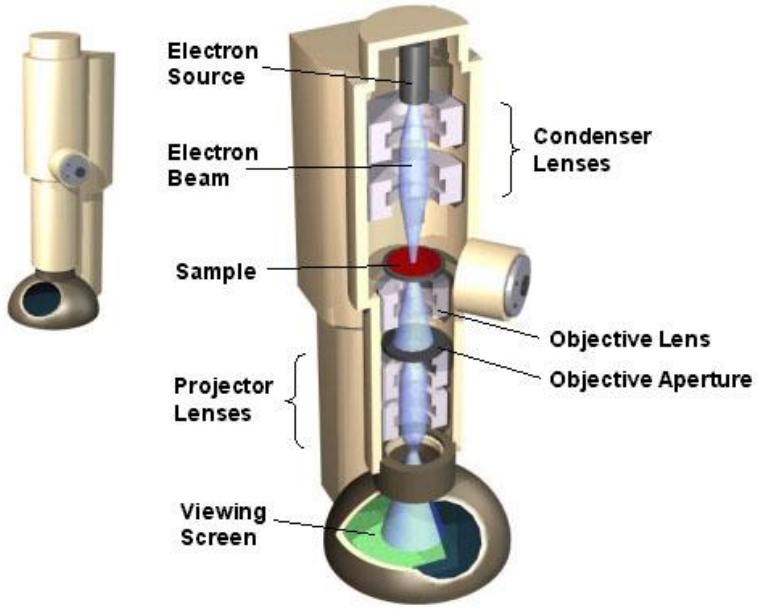

Figure 2. 6 Schematic of a transmission electron microscope (https://nanocomposix.com/products/tem-nanoparticle-analysis)

2.3.2 Dynamic Light Scattering (DLS)

Dynamic Light Scattering (DLS) is a tool for characterizing the size of GNPs in solution. DLS records the light scattered from a laser that passes through GNPs solution and then analyzes the modulation of the scattered light intensity as a function of time. As Brownian motion of GNP cause continually changes its configuration in the scattering volume (Wongtangprasert, 2012). Furthermore, larger particles would diffuse slower than smaller particles and the obtained information by measuring the time dependence of the scattered light to generate the rate of fluctuation that linked to a particle size (Figure 2.7). Moreover, Interpretation of DLS sizing data compared to Transmission Electron Microscopy images would determine from the aggregation state of the particles. If GNPs are agglomerated or having variability of the particle size in the solution, the DLS measurement is much larger than the TEM size. While, in an

unagglomerated solution, the diameter from DLS measurement would be similar the TEM size (Bantz et al., 2014).

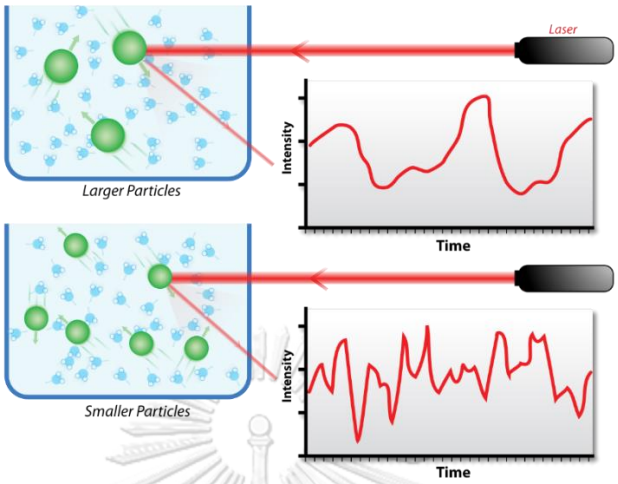

Figure 2. 7 Hypothetical dynamic light scattering of two samples: Larger particles on the top and smaller particles on the bottom (https://en.wikipedia.org/wiki/Dynamic_light_scattering)

2.3.3 Zeta Potential

Zeta Potential is a tool for understanding the state of the GNP surface and predicting the stability of the GNP in long term. Zeta Potential analysis is developed to determine the net surface charge of GNPs in solution which results in an increasing of ions that of opposite charge to the nanoparticle surface. So, the double layer of ions would exist around each particle as shown in Figure 2.8. When GNP moves, ions surrounded or within the boundary move with it. The potential that exists at the boundary is known as the Zeta potential which has values typically ranged higher than +30 mV and lower than -30 mV for prediction of the colloidal GNP stability (Clogston and Patri, 2011).

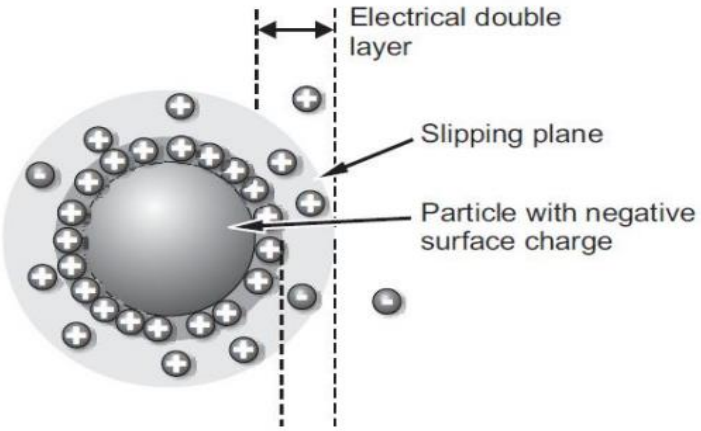

Figure 2. 8 Electric double layer surrounding nanoparticle (Clogston and Patri, 2011)

2.4 Acute lymphoblastic leukemia (ALL)

Acute lymphoblastic leukemia (ALL) is a cancer of blood cells which the bone marrow makes too many immature lymphocytes in the patients. Bone marrow is one of the important organ of the body to make immature blood cells that become subsequently mature blood cells. As shown in Figure 2.9, immature blood cells or blood stem cells may become a myeloid stem cell that makes red blood cells, platelets, and white blood cells or a lymphoid stem cell that makes a lymphoblast cell which may become one of three types of lymphocytes such as B lymphocytes, T lymphocytes, and natural killer cells. In ALL patient, too many immature blood cells become B lymphocytes or T lymphocytes. Unfortunately, these two types of lymphocyte are not well able to defend against infection like normal lymphocytes. Thus, theses nonfunctional lymphocytes become cancer cells or leukemia cells. ALL progresses rapidly and is generally fatal within months if left untreated (Marino and Fine, 2013). And its symptoms may include weakness, pale skin color, loss of appetite, fever, easy bleeding or bruising, bone pain or enlarged lymph nodes (Smith et al., 1996). Most common risk factors that cause ALL including exposure to x-rays before birth, past treatment with chemotherapy, and

especially having certain changes in genes. The research of Moellering et al., 2009, revealed that gene encoding human protein called NOTCH is often damaged in patients who have blood cell cancer, known as T-cell acute lymphoblastic leukemia (T-ALL) and discovered that using synthesized stapled peptide can suppress NOTCH activation in mice and also decrease cancer cell proliferation.

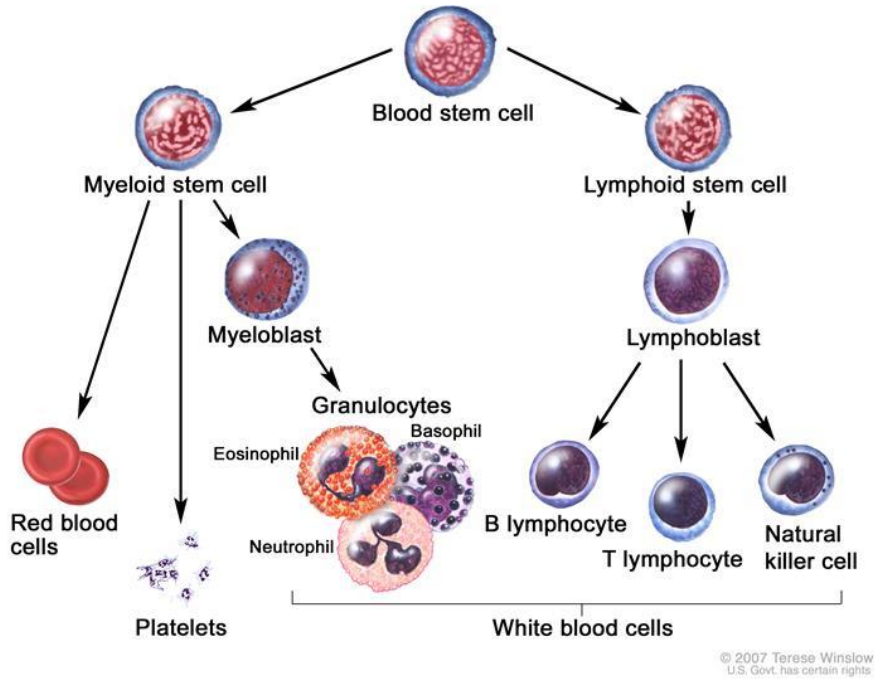

Figure 2. 9 Blood cell development
(Terese Winslow (illustrator), 2007)

2.5 NOTCH signaling pathway

NOTCH signaling involve in many processes such as morphogenesis, cellular proliferation, and programmed cell death. NOTCH signaling is started by binding of the extracellular domain of NOTCH to NOTCH receptor which consist of transmembrane, extracellular, and intracellular subunits (ICN). The ICN is released by γ-secretase activity that cleavage transmembrane domain into subunits. Then, ICN translocates to nucleus for interacting with transcriptional repressor CSL. Commonly, CSL regulates the transcriptional corepressor by binding and acting as a transcriptional

repressor (Nefedova et al., 2008). In contrast, binding of CSL with ICN create a shallow cavity along the interface of these two proteins. And this cavity is suitably bound by coactivator proteins of the mastermind-like (MAML) family. This ICN-CSL-MAML complex becomes a major factor to control transcription process that also activate NOTCH-dependent target genes. Normally, NOTCH signaling is controllable expression whereas the gain-of-function mutations in its pathway can cause cancer. Moreover, over fifty percent of T-ALL patients are caused by activating mutations in NOTCH pathway (Moellering et al., 2009). The efforts to counteract NOTCH pathway by blocking the production of ICN using small molecule called GSIs that can inhibit γ-secretase activity and these molecules also block many pathway downstream of γ-secretase activity. However, GSIs are not specific to NOTCH pathway that cause T-ALL patients treated with GSIs still suffer dose-limiting gastrointestinal toxicity which result from chronic blockage of NOTCH pathway (Riccio et al., 2008). Thus, the small peptide in stapled α-helical structure was synthesized to be regarded as promising novel anticancer agents.

2.6 Stapled α-helical peptides derived from mastermind-like 1 (SAHM1)

Stapled α-helical peptides derived from mastermind-like 1 (SAHM1) *is* a stabilized hydrocarbon-stapled α-helical peptide that targets a protein-protein interface and prevents assembly in the NOTCH activation complex and has structure that similarly to N-terminal side of dnMAML1 polypeptide forms (Figure 2.10) and shows the highest helicity value when compare to other forms. These reasons confirm that a staple fragment could prevent binding of full length MAML1 to ICN-CSL complex. The research of Moellering et al., 2009, reported that SAHM1 has a specific antagonistic effect on gene expression driven by NOTCH and its effect is observed

across a panel of human T-ALL cell lines like Jurkat. In addition, SAHM1 could target transcription factor of human NOTCH by binding to pre-assembled form of the CSL-NOTCH complex and competitive inhibition to MAML1 co-activator binding. These abilities of SAHM1 on NOTCH inhibition also cause prostate cancer cell death via induction of apoptosis in T-ALL cell.

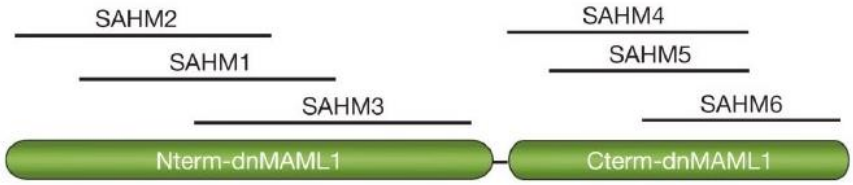

Compound	Sequence	Helicity
MAML1(21-36)	βA1a-ERLRRRIELCRRHHST	23%
SAHM1-UN	βA1a-ERLRRRI*LCR*HHST	40%
SAHM1	βA1a-ERLRRRI*LCR*HHST	94%
SAHM2	βA1a-SAVMERL*RRI*LCRRHH	73%
SAHM3	βA1a-RIELCRRHH*TCE*RYEAV	59%
SAHM4	βA1a-ERLELER*HTF*LHQR	67%
SAHM5	βA1a-ELER*HTF*LHQR	72%
SAHM6	βA1a-QHTFALH*RCI*AKAKR	56%
SAHM1-D1	βA1a-RELRREI*LCR*HHST	83%
SAHM1-D2	βA1a-RELRRRI*LCE*HHST	78%
dSAHM1	βA1a-DRLRRRM*NYR*RQTD	55%

Figure 2. 10 Design of MAML1-derived stapled peptides targeting CSL-NOTCH (Moellering et al., 2009)

2.7 Mode of program cell death

2.7.1 Apoptosis

In human body, there is a process as a homeostatic mechanism to maintain cell populations in tissues during development and aging known as apoptosis process. Apoptosis also occurs as a defense mechanism when cells are damaged by disease (Norbury and Hickson, 2001). Figure 2.11 shows the identification of the various morphological changes during apoptosis under light and electron microscopy. The obviously morphology can be observed that cells are shrink and smaller in size. Then, cell cytoplasm and chromatin is dense and DNA breaks into small piece and nucleus

begins to break apart while each organelle is more tightly packed. Afterward, the apoptotic cell would be phagocytosed by macrophage cells and degraded within phagolysosome. (Kurosaka et al., 2003).

The essential of apoptosis is no inflammatory reaction to other healthy cell even when the removal of apoptotic cell still occur. Because apoptotic cells do not release their cellular component into the surrounding tissue, they are quickly phagocytosed by surrounding cells involved in immune system to prevent secondary necrosis occurrence, and the engulfing cells do not produce anti-inflammatory cytokines (Savill and Fadok, 2000).

2.7.2 Necrosis

Necrosis is occured by the external factors such as trauma, toxin, and infection which cause detrimental to cell. Necrosis is a degradative process occured after cell death. Cell begins to swell and disrupt its organelle membrane. Then, its components release into extracellular compartment, which include many proteolytic enzymes that can cause inflammatory to surrounding tissue as shown in Figure 2.11. These initiate in the attraction of leukocyte and phagocyte cells to eliminate necrotic cells by phagocytosis. Moreover, the substances that are released by leukocyte cells would damage nearby healthy tissue and inhibit the healing process (Rock and Kono, 2008). In addition, the difference morphology between apoptosis cell death and necrosis cell death could be concluded as shown in Table 2.2.

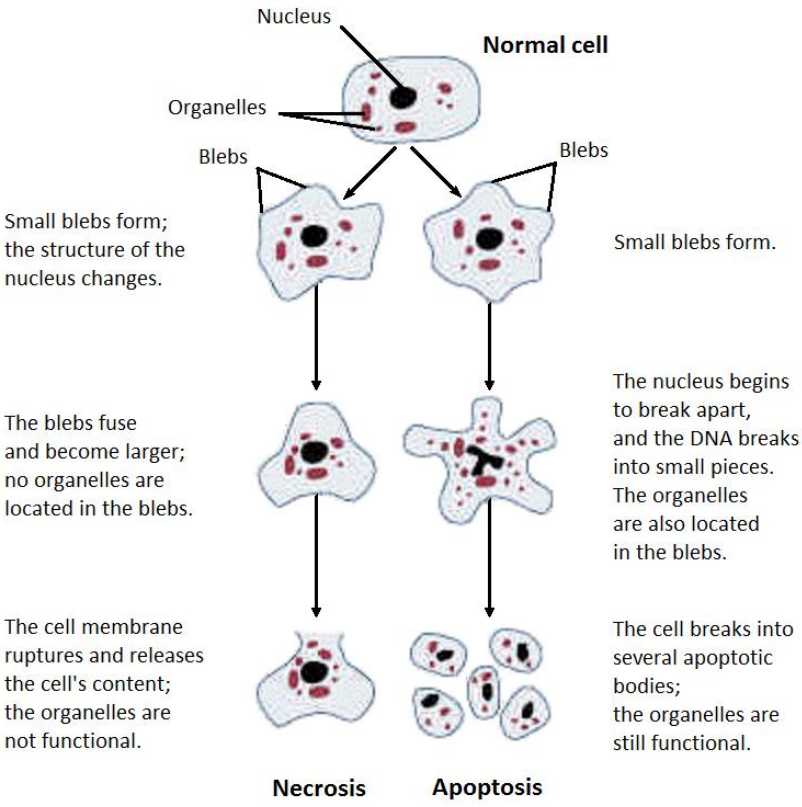

Figure 2. 11 Structural changes of cells undergoing necrosis or apoptosis.
(Source: http://pubs.niaaa.nih.gov/publications/arh25-3/175-184.htm)

Table 2. 2 Comparison of morphological features of apoptosis and necrosis.

Apoptosis	Necrosis
Single cells or small clusters of cells	Often contiguous cells
Cell shrinkage and convolution	Cell swelling
Pyknosis and karyorrhexis	Karyolysis, pyknosis, and karyorrhexis
Intact cell membrane	Disrupted cell membrane
Cytoplasm retained in apoptotic bodies	Cytoplasm released
No inflammation	Inflammation usually present

(Elmore, 2007)

2.7.3 Determination of apoptosis and necrosis cell death.

The patterns of cell death which are apoptosis and necrosis was determined by altering cell membrane that detected by dual staining dye, FITC conjugated Annexin V and propidium iodide (PI). The stained cells were investigated by flow cytometer, which is an important tool in cell sorting, biomarker detection, and cell counting. Flow cytometer be able to analyze more than thousand cells per second, in real time, by using electro detection to separate cells into single cell. Then, fluorescence intensity is measured and the quantity of apoptotic and necrotic cells are calculated at the same time. The result of the pattern cell death is shown in 4 quadrants that consist of necrosis, living cells, early apoptosis, and late apoptosis (Figure 2.12)**.**

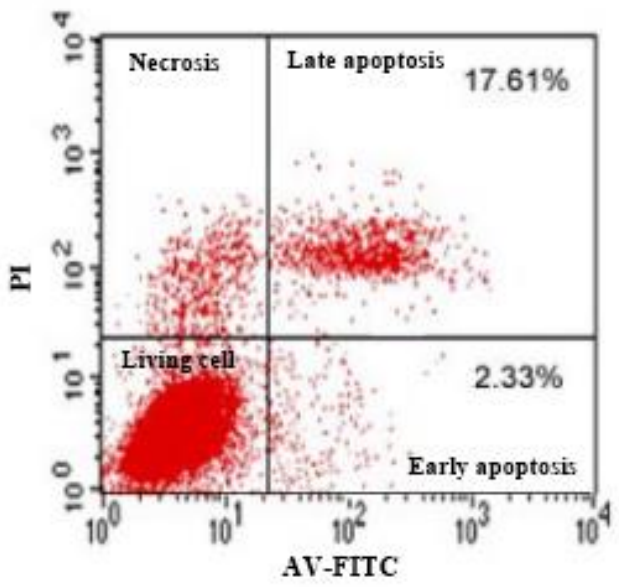

Figure 2. 12 Annexin V and PI staining
(C. Zhang et al., 2010)

Annexin V is generally used as dye to bind to phosphatidylserine, a marker of apoptosis, which is essential element of cell membrane. Phosphatidylserine would translocate from inner side of cell membrane to the surface and shows anionic

phospholipid properties that can attract the Annexin V which also has high affinity to bind and fluorochrome-labeled Annexin V can be detected by using flow cytometry. According to the research of Donghyun, 2016, they study the inducing apoptosis by using gold nanoparticles (AuNPs) conjugated with thiolated beta cyclodextrin (AuNP-S-β-CD). AuNP-S-β-CD-BC can inhibit the proliferation of cancerous MCF-7 cells via induction of apoptosis (Lee et al., 2016)

Propidium iodide (PI) is a red-fluorescence dye and bind specifically to DNA when it permeate into dead cells or only necrotic cells. This dyes makes possible to distinguish necrotic cell populations by flow cytometer. Necrosis pathway leading to cell death accompanied by cell swelling and cell membrane break down. The PI dye can easily get into necrotic cells to bind to its A-T rich of DNA fragment.

CHAPTER III

MATERIALS AND METHODS

3.1 Materials

3.1.1 Chemicals

Roswell Park Memorial Institute medium (RPMI1640)	Biochrom, Germany
Fetal calf serum (FCS)	Biochrom, Germany
3-(4,5-dimethylthiazol-2-yl)-2,5-diphenyltetrazolium bromide (MTT)	Bio Basic INC
Gold chloride trihydrate ($HAuCl_4$)	Sigma-Aldrich, USA
Sodium citrate	Sigma-Aldrich,USA
Thiolated methoxy polyethylene glycol (PEG), 5000	
Stapled α-helical peptides derived from mastermind-like 1 (SAHM1)	Merck, USA
FITC Annexin V and PI Apoptosis Detection Kit	Biolegend, USA
Dimethyl Sulfoxide (DMSO)	RCI labscan limited, Thailand
N-[N-(3,5-difluorophenacetyl)-L-alanyl] -S-phenylglycine t-butyl ester (μ)	Sigma-Aldrich, USA

3.1.2 Equipment

Flask 75 Filt	Nunc, Denmark
96-well plate and 6-well plate	Corning, New York
Centrifuge, model: universal 320	Hettich, Germany
Centrifuge, model: 5424 R	Eppendorf AG, Germany

37 ^{o}C and 5% CO_2 Incubator	Thermo Fisher scientific
Inverted fluorescent microscope	Nikon TMS
UV-visible spectrophotometer, model: Multiskan™ FC Microplate Photometer	Thermo Fisher scientific
Transmission Electron Microscope (TEM)	HT7700-Hitachi (120 kV)
Transmission Electron Microscope (TEM)	Jem-1400 (100kV)
Zetasizer	Malvern Instrument, UK
Flow cytometer, model: BD FACSCalibur™	Biosciences instruments
Larminar flow cabinet, model: HS 124	ISSCO

3.1.3 Cell line

Acute T-lymphoblastic leukemia Jurkat cells, clone E6-1, were obtained from the American Type *C*ulture Collection (Manassas, VA, USA; ATCC No. TIB-152™)

3.2 Methods

3.2.1 Preparation of gold nanoparticles

Gold nanoparticles were synthesized by citrate reduction method. (Modified from Turkevich et al., 1951). In a 250-mL Erlenmeyer flask equipped with a condenser, 49.5 mL DDI water was heated to boiling point with vigorous stirring. Then, 0.5 mL of 25 mM $HAuCl_4$ solution (1% by weight) was added. After refluxing for 10 min, 1 mL, 0.75 mL, and 0.5 mL of 40 mM of trisodium citrate was rapidly added as the reducing agent and capping agent (1% by weight) to the stirring solution for synthesis of gold nanoparticles 20 nm, 40 nm, and 60 nm in size, respectively. The color of the solution would change from a pale yellow to a wine-red color. Then, the solution was removed

from the heat and continue stirred for 15 min. After that, the solution was allowed to cool to room temperature. The solution was centrifuged twice at 10,000 rpm for 30 min to separate the particles and wash the remaining chemicals. The particles were suspended in distilled water and kept at 4 $^{\circ}$C for further use.

3.2.2 Characterization of gold nanoparticles

The position of the localized surface plasmon resonance (LSPR) band of the obtained colloidal gold nanoparticles was monitored by UV–Vis absorption spectrophotometry. The absorption spectrums were achieved in the range of 400–800 nm to check for maximum wavelength. Shape and size distribution of the particles were visualized by using transmission electron microscopy (TEM) and Image J analysis. Then, the particle size and zeta potential were measured by dynamic light scattering (DLS) to check for size and stability of the particle.

3.2.3 Preparation of SAHM1-gold nanoparticles conjugate (SAHM1-GNPs)

The preparation method of SAHM1-GNPs conjugate by using thiolated methoxy polyethylene glycol (thiolated PEG) average Mn 5,000 as a linker via a sulfur-gold bond was modified from Tkachenko's and Shim's method. (Shim et al., 2017; Tkachenko et al., 2005)

3.2.3.1 Preparation of SAHM1-thiolated PEG for conjugate on gold nanoparticle

Colloidal gold nanoparticle (200 µL) was added into 96-well plate. SAHM1 and thiolated PEG at the same concentration and volume were mixed in the ratio at one to one to obtain final concentration of 0 – 250 µM. Then, GNP was added into the mixture and incubated at room temperature for 1 h on shaking rotator. The mixture was then added with 80 µL of 10% NaCl to precipitate the excess GNPs. Finally, the mixture

was measured the absorbance at the maximum wavelength previously found from 3.2.2. The least concentration that show the highest absorbance was the optimum concentration of SAHM1-PEG.

3.2.3.2 Conjugation of SAHM1-thiolated PEG with gold nanoparticle

The solution mixture of SAHM1 and thiolated PEG at optimum concentration from 3.2.3.1 was added to 1 mL of GNP solution. The mixture was stirred at room temperature for 1 h to allow absolute exchange of thiol with citrate on the GNPs surface. Then, the mixture of SAHM1-GNPs was seperated using centrifugation at 12,000 rpm for 30 min. The supernatant was removed and the obtained SAHM1-GNPs pellet was resuspended in 1 mL of distilled water. Conjugation of SAHM1 and GNP as shown in Figure 3.1 was confirmed the shift in maximum wavelength (red shift) and stability which SAHM1-GNPs was kept for 1 and 3 weeks at 4 °C.

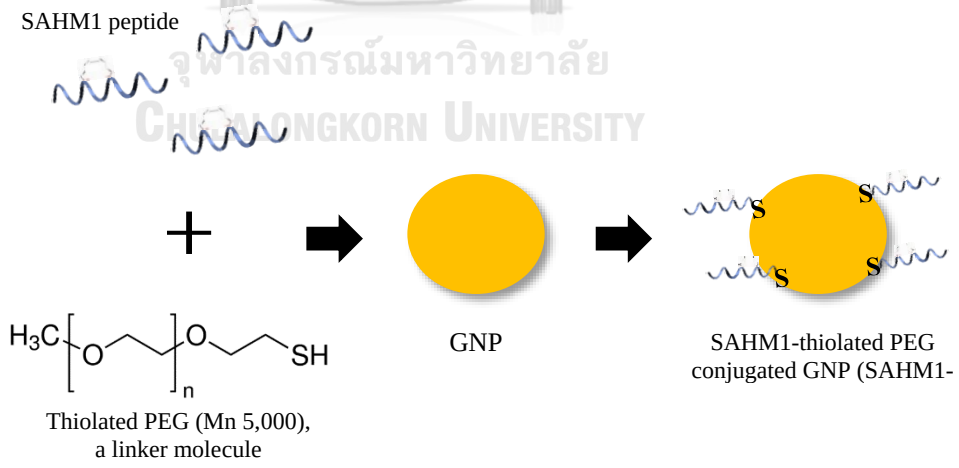

Figure 3. 1 Schematic illustration of GNP conjugated with SAHM1-thiolated PEG

3.2.4 Cell treatment condition

Acute T-lymphoblastic leukemia Jurkat cells (clone E6-1) was maintained in Roswell Park Memorial Institute medium (RPMI1640) with 10% FCS and incubated at 37 °C, 5 % CO_2 to attain 80 – 90% of cell confluence. Jurkat cells were counted and seeded at 5.0 x 10^4 cells/well in 96-well plates. Then, the cells were treated with different concentrations of GNPs, thiolated PEG, SAHM1, thiolated PEG-GNPs and SAHM1-GNPs at the optimum concentration found in 3.2.3.1. The plate was incubated for 24, 48 and 72 h at 37 °C in 5 % CO_2 atmosphere. Cells were also investigated the cytotoxicity assay, program cell death analysis and localization of SAHM1-GNPs.

3.2.5 Cytotoxicity assay

Antiproliferative activity was determined by cytotoxicity was studied by conventional MTT assay. The assessment of cell metabolic activity was performed by adding 10 µL of 5 mg/mL MTT in normal saline solution (NSS) and incubating at 37 °C in 5 % CO_2 atmosphere for 4 h. Then, the MTT solution was discarded and 150 µL of 100% DMSO solution was added into each well to dissolve the purple formazan crystals. The optical density was then read at 540 nm by using a microplate reader spectrophotometer. The percentage of viable cell was calculated using the following equation:

$$\% \text{ Cell viability} = \frac{\text{Experimental OD at 540 nm}}{\text{Control OD at 540 nm}} \times 100$$

Cells treated with 1%DMSO were used as a control. Data obtained can be used for IC50 evaluation by plotting the concentration versus the percentage of cell viability.

3.2.6 Apoptosis analysis

After cytotoxicity assay, concentration of SAHM1-GNPs that showed the highest antiproliferative activity against Jurkat cells was selected to analyze its effect on types of program cell death. The percentage of cell was measured using a flow cytometer.

Jurkat cells were cultured in 12-well plate at 2.5 x 10^5 cells/well. After 24 h of incubation to attain 80 – 90% of cell confluence. Cells were treated at the condition which showed the lowest percentage of viable cells for 24 – 72 h of incubation. In addition, 50 µM DAPT was a positive control and Jurkat cell without treatment was a negative control. Cells were then harvested at about 10^6 cells/well, centrifuged at 2,000 rpm for 5 min and discarded the supernatant. Cells were washed by 20 mM PBS buffer (5 mL) containing 1% FCS and centrifuged again to precipitate cells. Then, the precipitate was resuspended in cold 20 mM PBS buffer (0.5 mL) containing 1% FCS and placed on ice. Next, FITC Annexin V Apoptosis Detection Kit with PI was used to analyze the program cell death of these cells.

Cell suspension was centrifuged at 2,000 rpm for 5 min to collect cells and the supernatant was removed. Then, cells were added with 300 µL of Annexin V binding buffer only for untreated cell condition (negative control) while 100 µL of Annexin V binding buffer and 5 µL of FITC conjugated Annexin V solution were added to the positive control and SAHM1-GNPs condition. Next, cells were incubated on ice for 10 min in the dark. After that, cells were added with 100 µL of Annexin V binding buffer and 10 µL of PI solution. Finally, the mixture was pipetted into 12 x 75 mm polystyrene test tubes and analyzed with the BD FACSCalibur™ flow cytometer

3.2.7 Intracellular distribution of gold nanoparticles

To study the dynamic intracellular distribution of GNPs, 1 x 10^6 Jurkat cells were cultured in 6-well plate for overnight. GNPs and SAHM1-GNPs at the concentration that showed the highest antiproliferative activity found in 3.2.5 were then applied to the cells and incubated for 24 h at 37 $^{\circ}$C, 5 % CO_2. After that, phosphate buffer saline (PBS) was used to wash the cells twice. Cells were fixed with cold 2.5% glutaraldehyde in 0.1 M sodium cacodylate buffer before embedding them in closed grid. Ultrathin sections of the cell samples were cut and observed with Transmission Electron Microscope (Jem-1400). The intracellular location of the samples was then analyzed.

3.2.8 Statistical analysis

Each experiment was determined in triplicate and the data were showed as mean ± standard deviation. Different among group was performed using the SPSS program and analyzed by one-way analysis of variance (ANOVA). The multiple comparisons were then analyzed by Duncan test. Differences were considered significant at $p < 0.05$.

CHAPTER IV

RESULTS AND DISCUSSIONS

GNPs have been used in the area of medical for centuries due to their lack of toxicity, rich chemical surface and easy synthesis. They have been proven to be an excellent carrier for conjugation and then delivering several biomolecules to the target site (Giljohann et al., 2010). In this thesis, effect of GNPs on the antiproliferative activity of SAHM1 peptide was studied in Jurkat cell line. SAHM1 peptide was attached onto the surface of GNPs (at three different sizes of 20 nm, 40 nm and 60 nm) using thiolated polyethyleneglycol (thiolated-PEG) as the linker. Jurkat cells were treated with the SAHM1-GNP at different conditions as compared to the untreated cells. Cell viability and program cell death of the treated cells were investigated.

4.1 Preparation and characterization of gold nanoparticles

4.1.1 Synthesis of GNPs

GNPs were synthesized by the chemical reaction between trisodium citrate and tetrachloroauric acid ($HAuCl_4$). Three different ratios of citrate to $HAuCl_4$ were used to prepare GNPs in order to obtain three different sizes (20, 40 and 60 nm) of GNPs (Kumar et al., 2012). Figure 4.1 showed GNP solutions prepared by mixing 0.5 mL of 25 mM $HAuCl_4$ with 40 mM trisodium citrate at (A) 1.0, (B) 0.75 and (C) 0.5 mL. The color was red wine and the intensity showed tendency to inversely vary with the volume of the citrate used in the reaction.

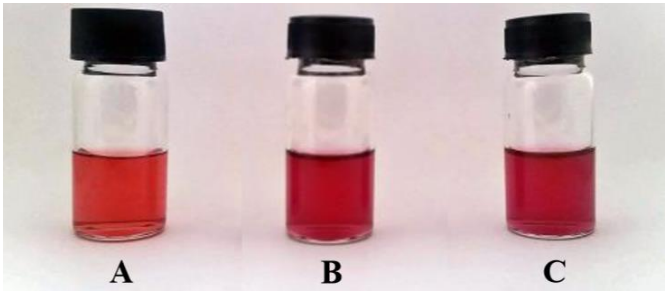

Figure 4. 1 Color of GNP solutions prepared by mixing 0.5 mL of 25 mM $HAuCl_4$ with 40 mM trisodium citrate at the volume of (A) 1.0 mL, (B) 0.75 mL and (C) 0.50 mL

UV-Vis spectrum of the reaction mixtures were shown in Figure 4.2 It could be seen that the maximum wavelength (λ_{max}) of each reaction solution was different. The reaction with 1.0, 0.75 and 0.5 mL of citrate gave the λ_{max} at 520, 525 and 530 nm, respectively, thus suggesting that size of the GNP in the three solutions were different. It has been suggested that UV-Vis spectrum of the GNP solution can be used to tell the size and the colloidal state of the particles (Khlebtsov, 2008). Interaction between the GNPs and light is strongly dictated by size and dimension of the particles. The light causes a concerted oscillation of electron charge around GNPs that is in resonance with the frequency of the visible light. These resonant oscillations are known as surface plasmon resonance (Anker et al., 2008). Moreover, it had been reported that the surface plasmon resonance of the particle sizes from 20 to 100 nm is clearly visible as a peak in the range between 520 and 580 nm (Haiss et al., 2007).

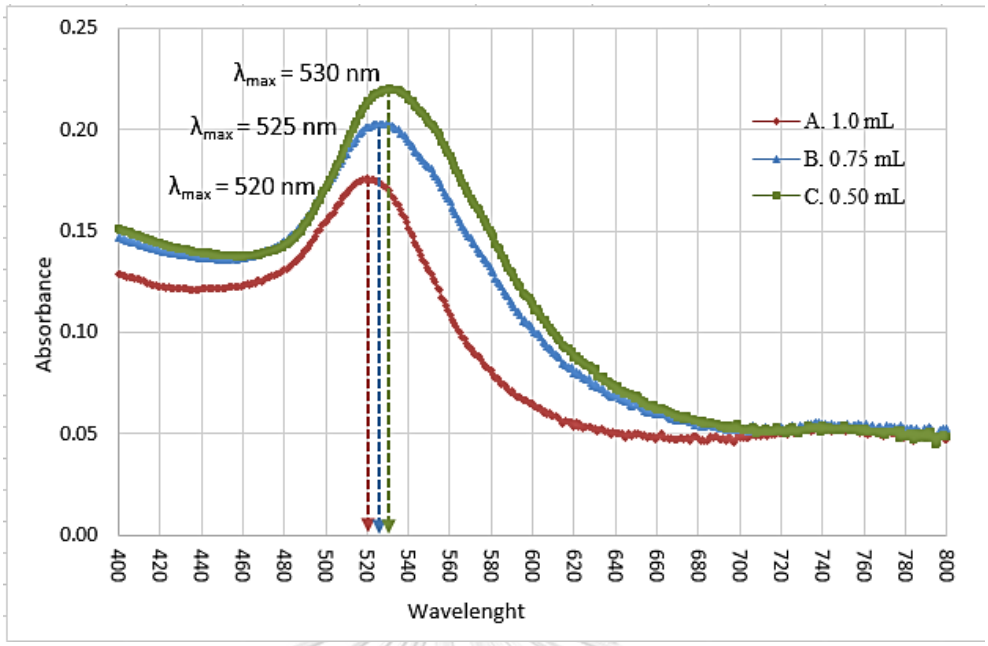

Figure 4. 2 UV-Vis spectrum of GNP solutions prepared by mixing 0.5 mL of 25 mM $HAuCl_4$ with 40 mM trisodium citrate at the volume of (A) 1.0 mL, (B) 0.75 mL and (C) 0.50 mL

In addition, UV-Vis spectrum of the GNP solution could be used to evaluate the particle stability which is a necessary parameter for biomedical applications. Spectrum of the GNP solutions kept at 4 °C for one and three weeks were shown in Figure 4.3. It could be observed that the λ_{max} of the solutions were not shifted as compared to those of freshly prepared solutions presented Figure 4.2. Moreover, the peaks in all cases, showed a symmetric bell shape. These indicated that the GNPs were in a well stabilized colloidal phase.

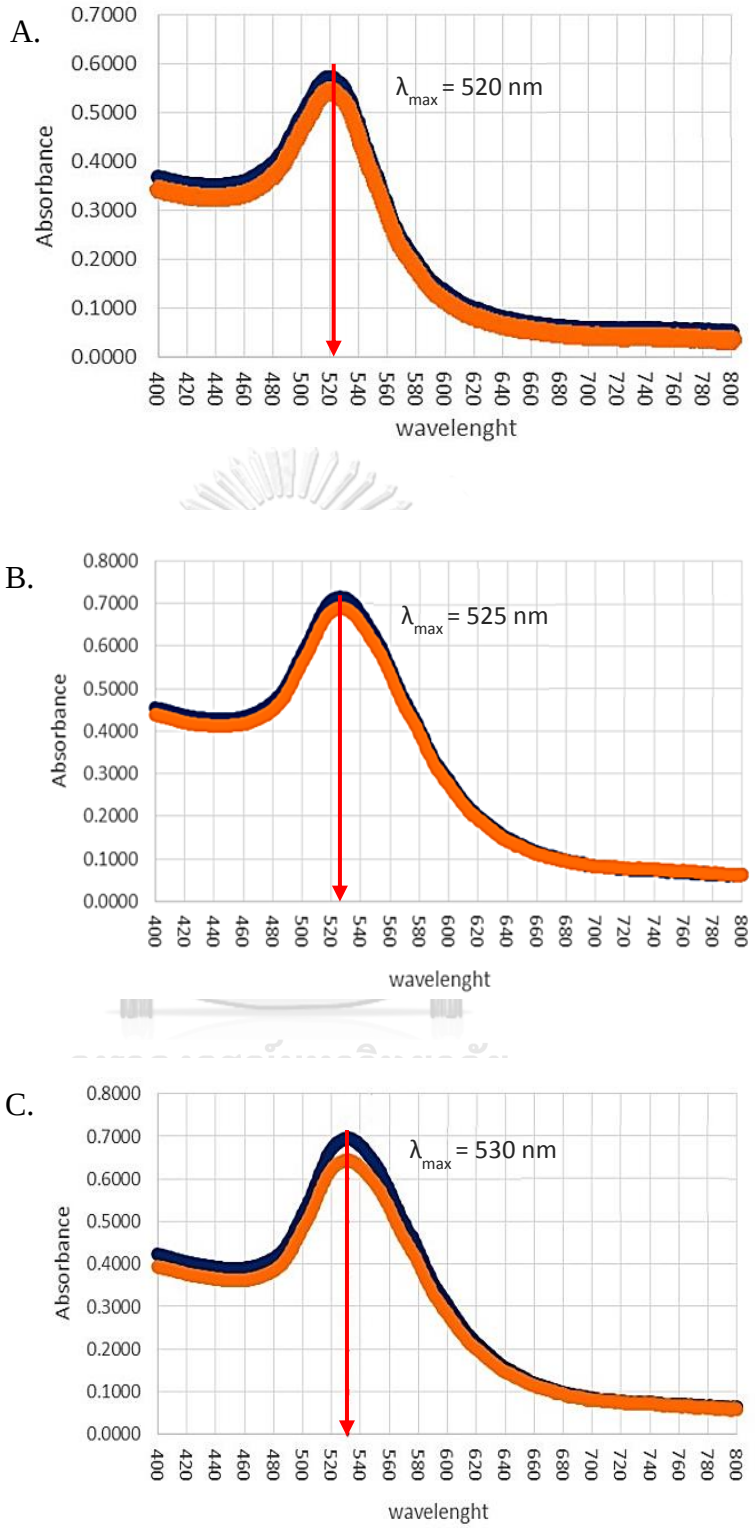

Figure 4. 3 UV-Vis spectrum of GNP solutions kept at 4 °C for 1 week, (—●—) and 3 weeks, (—●—) after preparation by mixing 0.5 mL of 25 mM $HAuCl_4$ with 40 mM trisodium citrate at the volume of (A) 1.0 mL, (B) 0.75 mL and (C) 0.50 mL

4.1.2 Size of the prepared GNPs

Transmission electron microscopy (TEM) was used to identify uniformity, morphology and size distribution of GNPs. As shown in Figure 4.4, the morphology of the particles was rather spherical in shape and the particle were in well-dispersed state. Size distribution of the GNPs prepared at different conditions was calculated by Image J analysis software. The reactions between 0.5 mL of 25 mM $HAuCl_4$ and 40 mM trisodium citrate at 1.0, 0.75 and 0.5 mL yielded the GNPs in the size range of (A) 15-20 nm, (B) 40-45 nm and (C) 60-65 nm, respectively (Figure 4.4). In addition, it could be noticed that size distribution of the GNPs was uniform in size for the case of 15-20 nm which presented at 70% of the total particles. On the contrary, for the larger sizes, the GNPs were not uniform in size. Only 35-40% of the particles were in the expected size range.

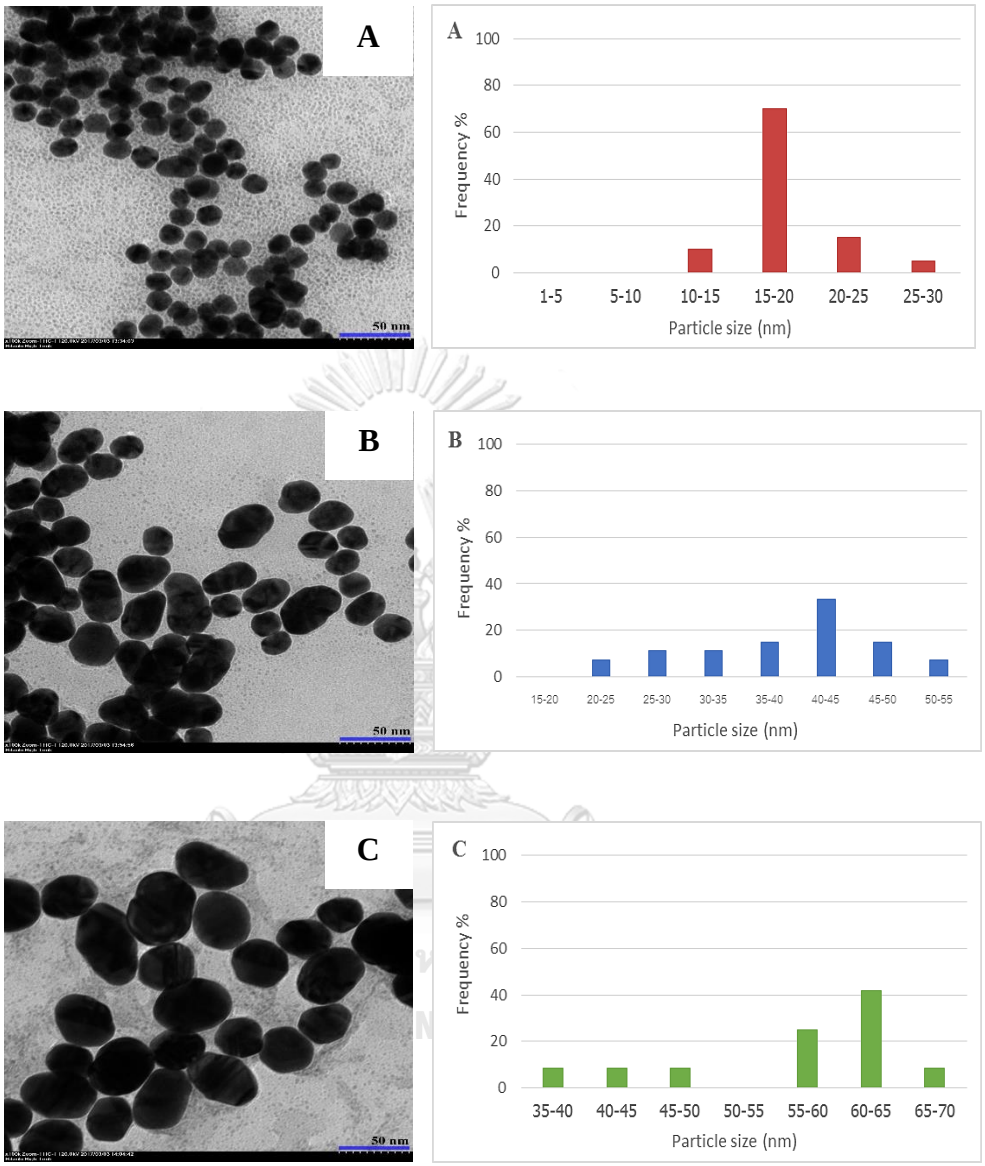

Figure 4.4 TEM images and size distribution analysis of GNPs prepared by mixing 0.5 mL of 25 mM $HAuCl_4$ with 40 mM trisodium citrate at the volume of (A) 1.0 mL, (B) 0.75 mL and (C) 0.50 mL

4.1.3 Surface charge of the prepared GNPs

Surface characteristics of the GNPs greatly affect the properties of the particles. Surface charge measured in a term of zeta potential has been used to indicate the stability of the particles. Particles with the zeta potential value > +30mV or < -30 mV are considered to be stable particles because particles with strongly positive or negative charges would repel each other, thus preventing them from aggregation (Tripathi et al., 2012). Zeta potential values of the prepared particles were quantified and shown in table 4.1. The result showed that the zeta potential values of the prepared GNPs from the three conditions were less than -30 mV, indicating that the obtained GNPs were stable and would not aggregate for a certain period.

Table 4.1 Zeta potential of gold nanoparticle

Gold nanoparticle (nm)	Zeta potential (mV)
20 nm	-39.37 ± 0.06
40 nm	-38.76 ± 0.23
60 nm	-35.67 ± 0.06

4.2 Preparation of SAHM1-GNPs

In order to attach SAHM1 onto the GNPs, thiolated polyethylene glycol (thiolated PEG) was used as the linker between SAHM1 and the GNPs. SAHM1 peptide was mixed with thiolated PEG at the equal molar ratio to obtain 1:1 linkage. Subsequently, various concentrations of SAHM1-thiolated PEG conjugate were mixed with the GNPs to find the optimum concentration of SAHM1-thiolated PEG that could

cover the surface and prevent aggregation of the GNPs. Figure 4.5 showed the absorbance values at the λ_{max} of the GNP solutions mixed with various concentrations of the SAHM1-thiolated PEG. It could be seen that color of the solution was grayish at the lower concentration of the SAHM1-thiolated PEG and was reddish at the higher concentration of the SAHM1-thiolated PEG. This could be due to the fact that at low concentration, the amount of SAHM1-thiolated PEG was not high enough to cover the surface and prevent the GNPs from aggregation. As a result, grayish color of the aggregated particles could be observed. On the contrary, at high concentration, the amount of SAHM1-thiolated PEG was high enough to create surface environment that the aggregation of the particles could not occurred. Therefore, reddish color of the colloidal GNP solution could be observed. From the relation between the absorbance value and the concentration of SAHM1-thiolated PEG shown in Figure 4.5, it could be concluded that the optimum or the least concentration of SAHM1-thiolated PEG required for the preparation of SAHM1-GNPs was 62.5 µM for all three sizes of the prepared GNPs.

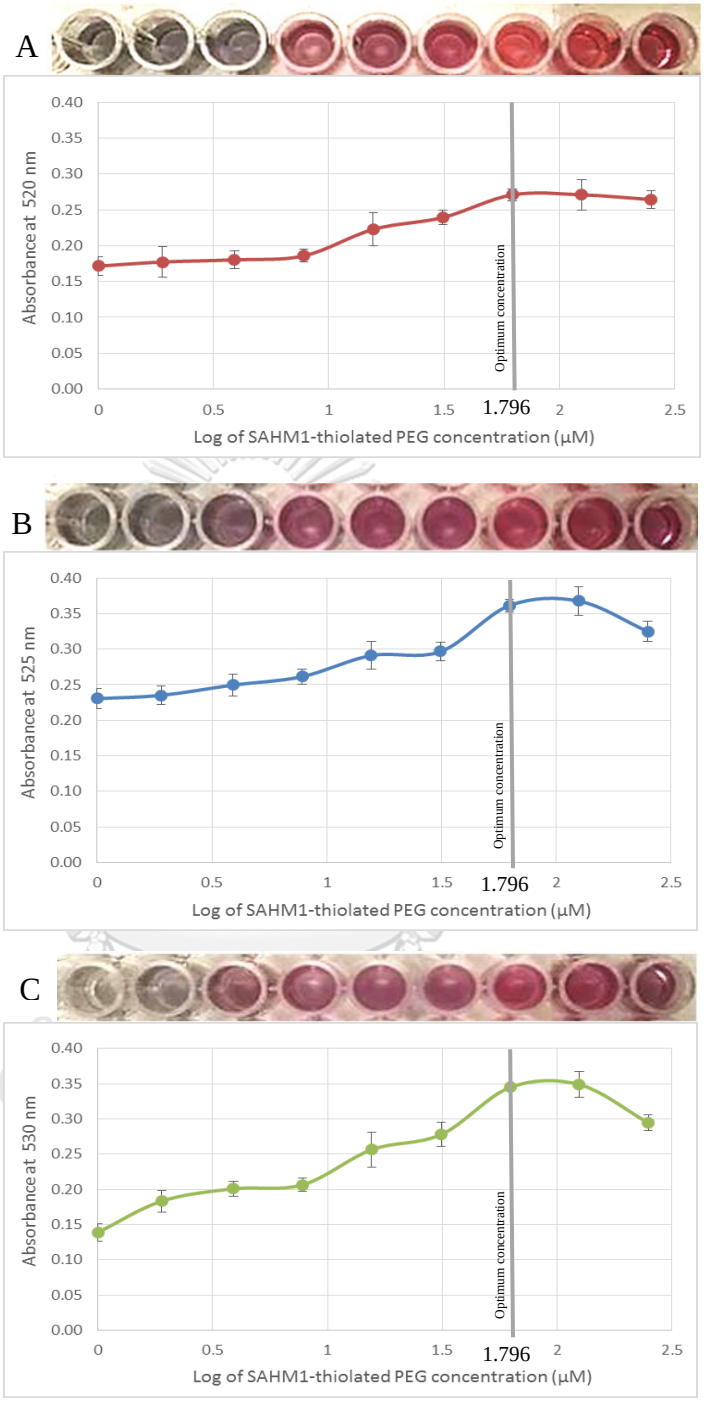

Figure 4.5 Color and absorbance measured at the λ_{max} of the of SAHM1-GNP solution prepared at various concentrations of SAHM1-thiolated PEG using (A) 20 nm GNPs, (B) 40 nm GNPs and (C) 60 nm GNPs

In addition, it has been known that GNPs express unique optical and physical properties depending on their size, shape and surface structure. The spectral position of the localized surface plasmon resonance indicating a distinct optical feature of the GNPs are depended on shape and size of the GNPs (Juvé et al., 2013). Therefore, after surface modification of the GNPs with biomolecules, UV-Vis spectroscopy was used as a basic technique to indicate the change on the particle surface. UV-Vis spectrum of the SAHM1-GNPs solutions were shown in Figure 4.6. It could be seen that the red-shift in the λ_{max} of the spectrum of the SAHM1-GNPs was occurred as compared to those of the GNPs. The λ_{max} was 528 nm, 531 nm and 536 nm for the SAHM1-GNPs with the averaged size of 20 nm, 40 nm and 60 nm, respectively while the λ_{max} of the unmodified GNPs was 520, 525 and 530 nm, respectively.

A.

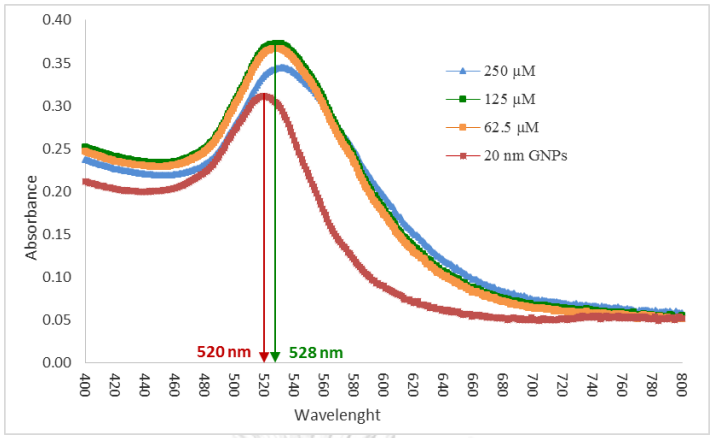

B.

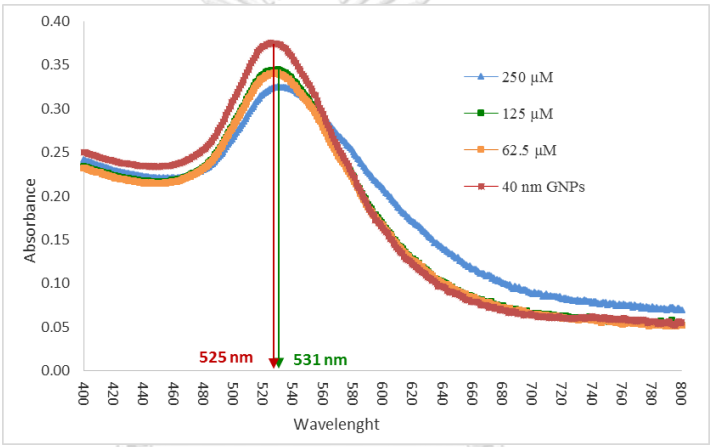

C.

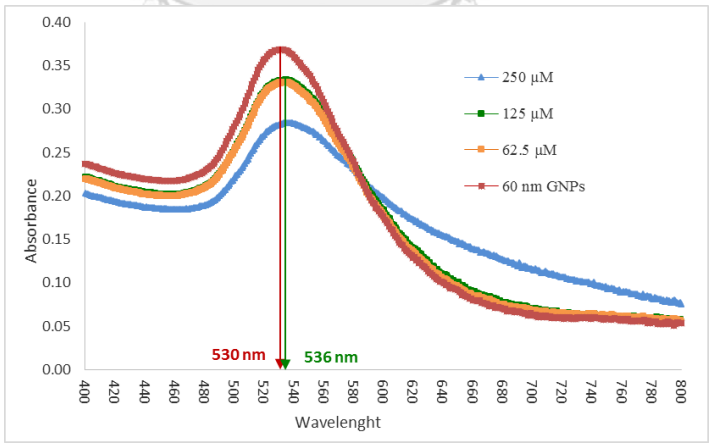

Figure 4.6 UV-Vis spectrums of GNP solution and SAHM1-GNP solution prepared by the averaged GNP size of (A) 20 nm, (B) 40 nm and (C) 60 nm and SAHM1-thiolated PEG conjugate at the concentration of (—■—) 62.5 µM, (—■—) 125 µM and (—▲—) 250 µM

4.3 Antiproliferative activity of SAHM1-GNPs

4.3.1 Cytotoxicity assay

The effect of GNPs and thiolated PEG used as the carrier and the linker of SAHM1 on the cell viability of Jurkat leukemic T-cell line was studied. After treatment for 24, 48 and 72 h, MTT assay was performed to attain cell viability. The percentage of cell viability at the different conditions of treatment was shown in Figure 4.7. The untreated cells were used as the control while the cells treated with gamma (γ)-secretase inhibitors (DAPT) drug were used as the positive control. Interestingly, both GNPs and thiolated PEG were slightly toxic to the Jurkat cells. There was a tendency that in case of the GNPs, toxicity varied inversely with the size of the particles while in case of the thiolated PEG, toxicity varied with respect to the concentration. However, in all cases, cell viability was higher that 75%. These findings were not in agreement with those findings reported that GNP (Pan et al., 2007) and thiolated PEG (Manohar et al., 2009) was not toxic. This could be due to the reason that different cell line used in the treatments was different. Each cell line might have different threshold level in order to tolerate the toxicity of the GNPs and the thiolated PEG.

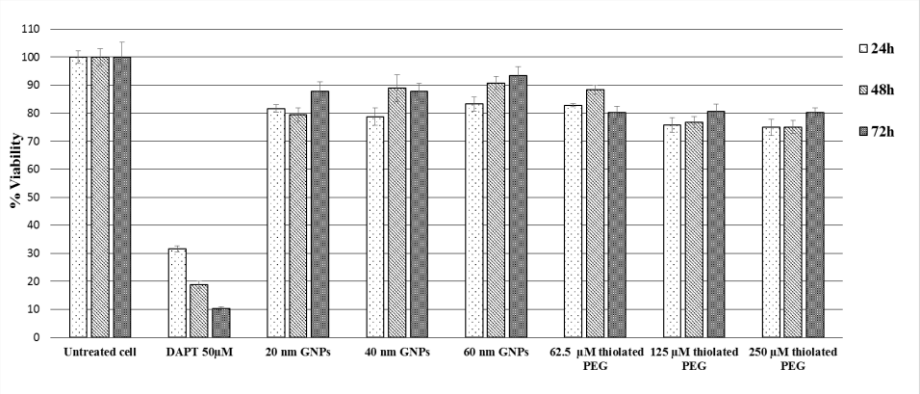

Figure 4.7 Cell viability of Jurkat cells treated with GNPs or thiolated PEG. Data are the mean±SD of three independent experiments of three replicates.

In addition to the toxicity of the GNPs and the thiolated PEG, that of thiolated PEG-GNP conjugate was also studied as shown in Figure 4.8. It could be noticed that the thiolated PEG-GNP conjugate was more toxic than the GNPs and the thiolated PEG. This could be the combination of toxicity of the two components. It could be seen that at the same concentration of the thiolated PEG, the toxicity of the conjugate varied with respect to the size of the GNPs. In case of 20 nm GNPs, the toxicity of the conjugate varied with the thiolated PEG concentration where as in case of 40 and 60 nm GNPs, the toxicity varied inversely with the thiolated PEG concentration. These findings were different from the previous findings described above. However, as mentioned earlier, properties of the GNPs depended on the surface properties and size of the particles. Modification of the GNP surface with thiolated PEG could change the toxic properties of the GNPs.

A

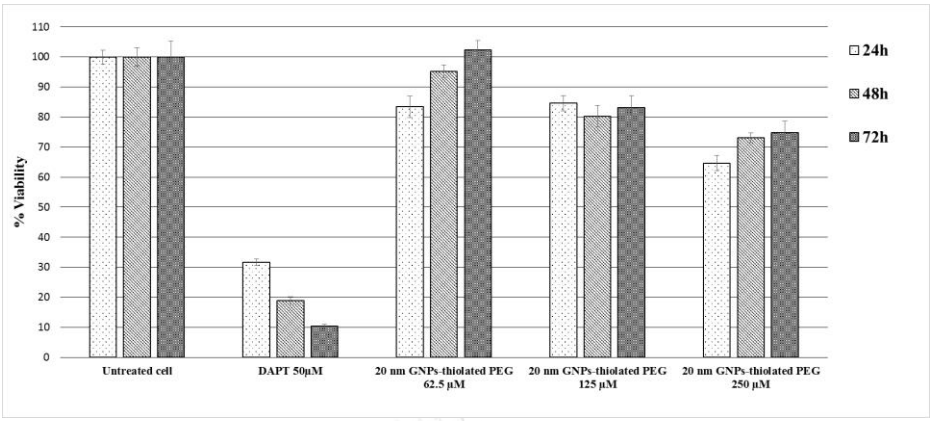

B

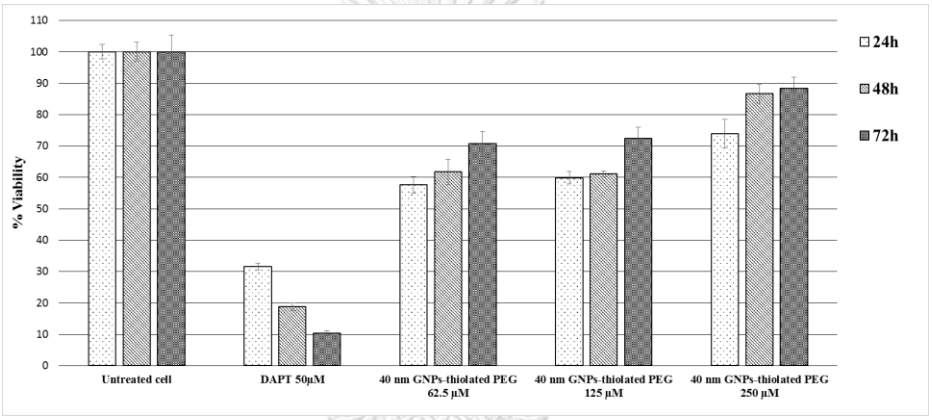

C

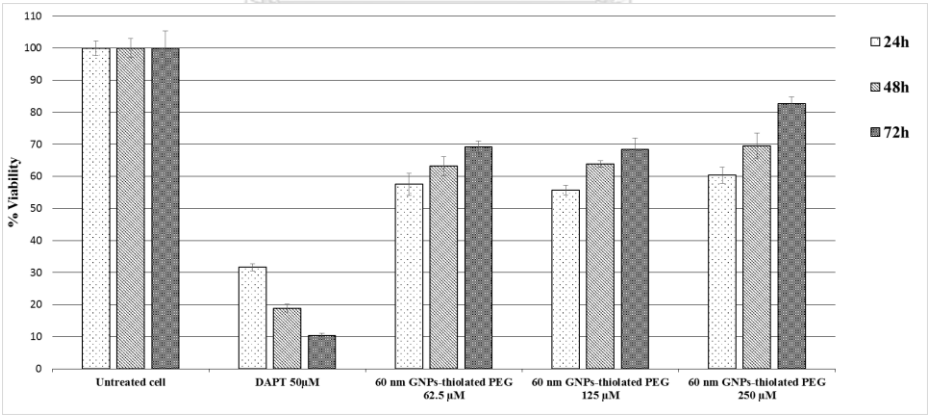

Figure 4.8 Cell viability of Jurkat cells treated with GNPs-thiolated PEG for 24 h (⬚), 48 h (▨) and 72 h (▩) using GNPs at the average size of (A) 20 nm, (B) 40 nm and (C) 60 nm. Data are the mean±SD of three independent experiments of three replicates.

Attachment of SAHM1 to thiolated PEG-GNPs might also affect the toxicity of the particles. Cell viabilities of Jurkat cells treated with SAHM1 and SAHM1-GNPs linked by thiolated PEG were shown in Figure 4.9. It could be clearly seen that, in most conditions, cell viabilities of Jurkat cells treated with SAHM1-GNPs were lower than those of the cells treated with SAHM1. Especially, cell viabilities of the cells treated with 62.5 µM and 125 µM SAHM1-GNPs (20 nm) were clearly lower than those of the cells treated with SAHM1 or with thiolated PEG-GNPs. However, in other cases, as also compared to those presented in Figure 4.8, it was not obvious that the decreases in cell viability were due to SAHM1 which was attached to the thiolated PEG-GNPs. The cell viability values of the cells treated with SAHM1-GNPs were approximately at the same level of those treated with thiolated-GNPs. Furthermore, it could be noticed that, in most cases, cell viability values of the cells treated for 72 h were higher than those of the cells treated for 24 h. It was possible that Jurkat cells could adjust cell conditions to tolerate or reduce the effect of both SAHM1-GNPs and thiolated PEG-GNPs. The survived cells were able to grow in these conditions. These results indicated that enhancement of antiproliferative activity of SAHM1 by using the thiolated-PEG-GNPs as the carrier was not clearly obtained for all condition tested. This could be due to the reason that to obtain the antiproliferative activity, SAHM1 should be released from the particles and be in the free form so that it could be recognized by the binding partner, thus significantly decreasing the cell viability.

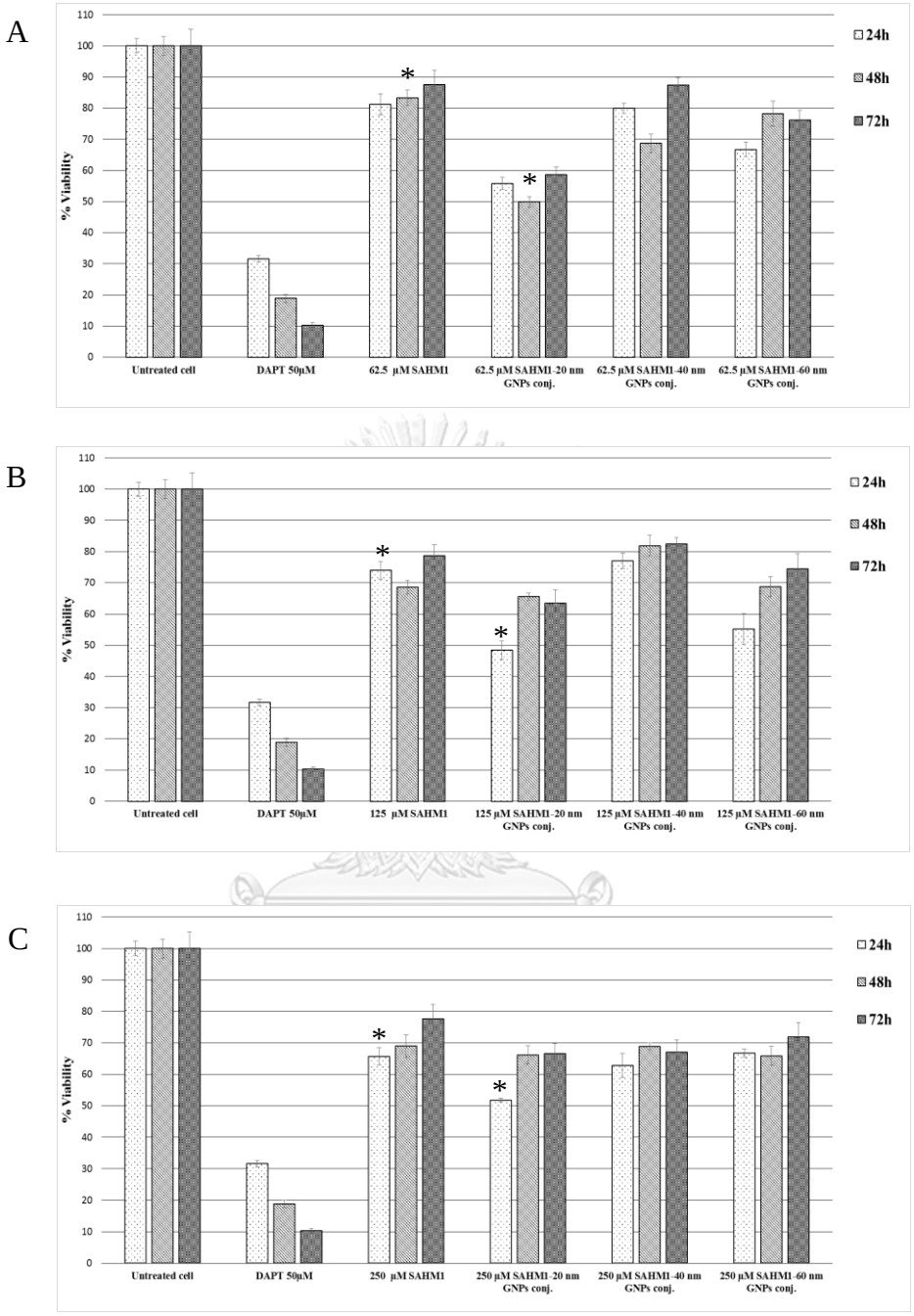

Figure 4.9 Cell viability of Jurkat cell after 24, 48 and 72 h treatments with different concentrations of SAHM1-GNPs: (A) 62.5 μM, (B) 125 μM, and (C) 250 μM**.** Data are the mean±SD of three independent experiments of three replicates. * denotes a statistically significant difference from the GNPs analyzed by ANOVA with $P<0.05$.

4.3.2 Effect of SAHM1-GNPs on morphology of Jurkat cells

Morphology of Jurkat cell after treatment with 62.5 μM SAHM1-GNPs (20 nm) for 48 h was observed under inverted fluorescent microscope (Figure 4.10). It could be seen that the untreated cells (A) were round in shape and healthy grown in clumps. Like untreated cells, cells treated with GNPs at 20 nm (B), 62.5 μM thiolated PEG (C), 62.5 μM thiolated PEG-GNPs 20 nm (D) and 62.5 μM SAHM1 (E) were healthy. In contrast, cells treated with 62.5 μM SAHM1-GNPs 20 nm (F) were larger than normal, and irregular in shape.

These results indicated that thiolated PEG and GNPs could be used as linker and carrier to conjugate with SAHM1 so that the SAHM1-GNPs conjugate would toxic to Jurkat cells. This finding were in accordance with a previous research showing efficiently binding of peptides-thiolated PEG to GNPs resulted in greater stability leading to more toxic to cancer cells (Yang et al., 2018).

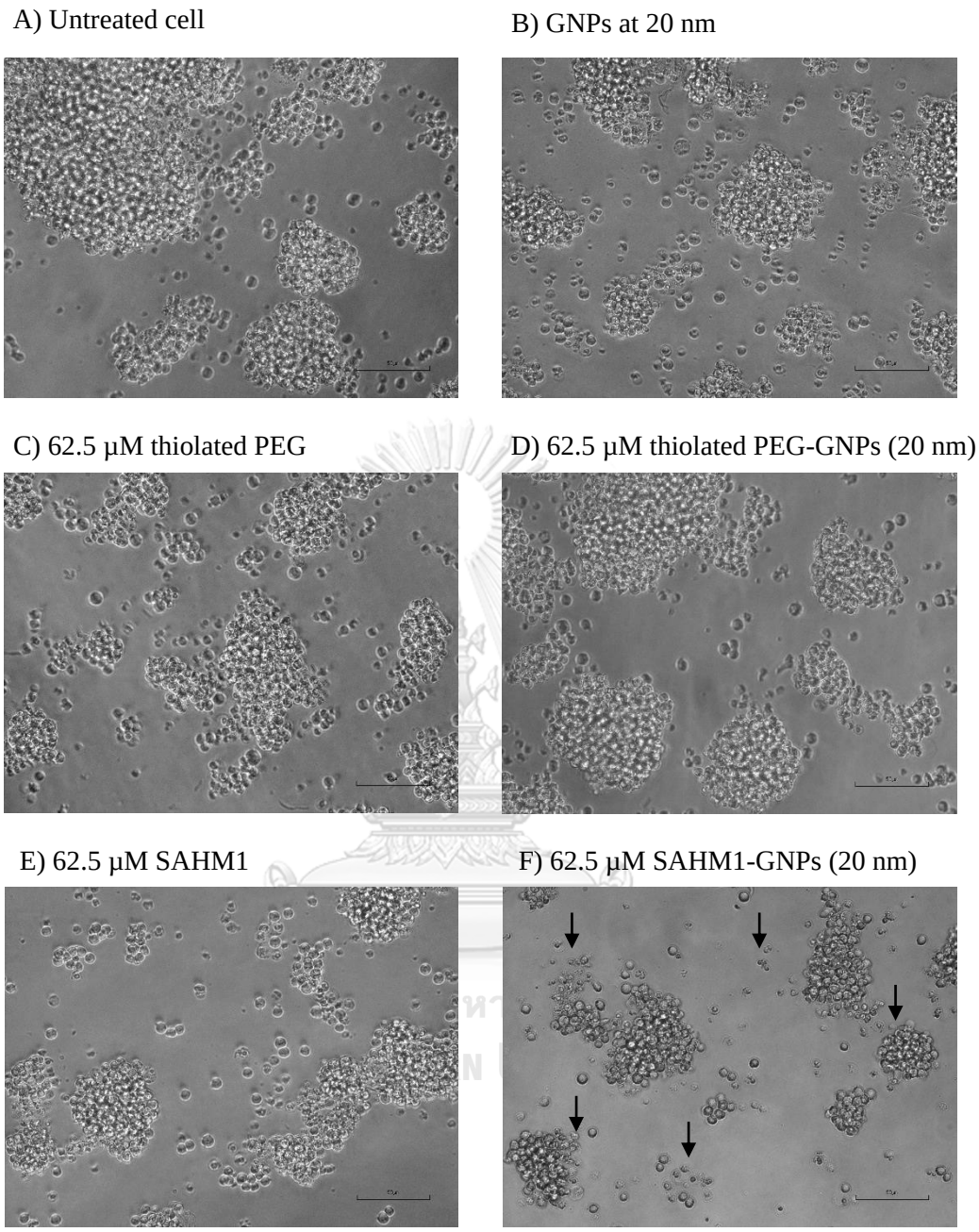

Figure 4. 10 Morphology of Jurkat cells treated with (A) Untreated cell, (B) GNPs at 20 nm, (C) 62.5 µM thiolated PEG , (D) 62.5 µM thiolated PEG-GNPs (20 nm), (E) 62.5 µM SAHM1 and (F) 62.5 µM SAHM1-GNPs (20 nm). All images were magnified 20X and the scale bar was 50 µm. A black arrow indicated unhealthy cell.

4.3.3 Analysis of program cell death

Since Jurkat cells treated with 62.5 µM SAHM1-GNPs (20 nm) yielded lowest cell viability, cells from this condition were selected to be studied for program cell death by flow cytometry. After treatment with SAHM1-GNPs for 24 h and 48 h using DAPT as the positive control, cells were stained with Annexin V and propidium iodide. Fluorescence signal was detected and analyzed by flow cytometer. The analysis shown in Figure 4.11 and 4.12 revealed that fluorescence signals were in quadrant 2 and 4, indicating that cell death was induced by early and late apoptosis stage. Moreover, the percentage of Jurkat cells in each quadrant of the profile was calculated and investigated as shown in Figure 4.13. It was found that more than 70% of the cell treated with SAHM1-GNPs were most died in early and late apoptosis as can be clearly seen in Figure 4.13 (B). The effect of this conjugate on program cell death was similarly to the finding which has been reported that using herceptin-GNPs conjugate effectively induce breast cancer cell apoptosis via receptor-mediated endocytosis interaction (Rathinaraj and Al-Jumaily, 2015).

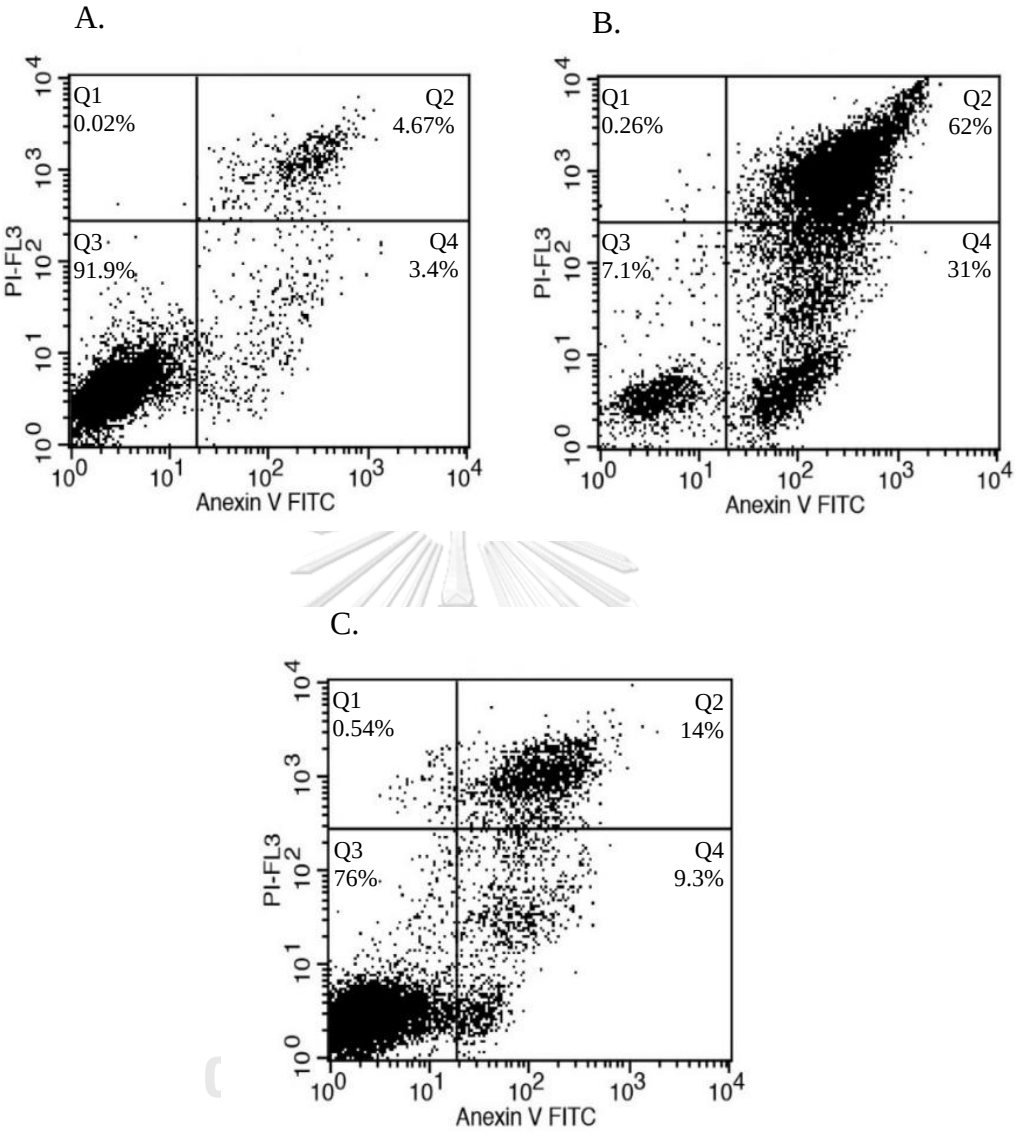

Figure 4. 11 Flow cytometry profile of Jurkat cell. A: untreated cell stained, B: cells treated with 50 µM DAPT (positive control), C: cells treated with 62.5 µM SAHM1-GNPs (20 nm) for 24 h. Quadrant 1 (Q1): necrosis, quadrant 2 (Q2): late apoptosis, quadrant 3 (Q3): live cell, quadrant 4 (Q4): early apoptosis

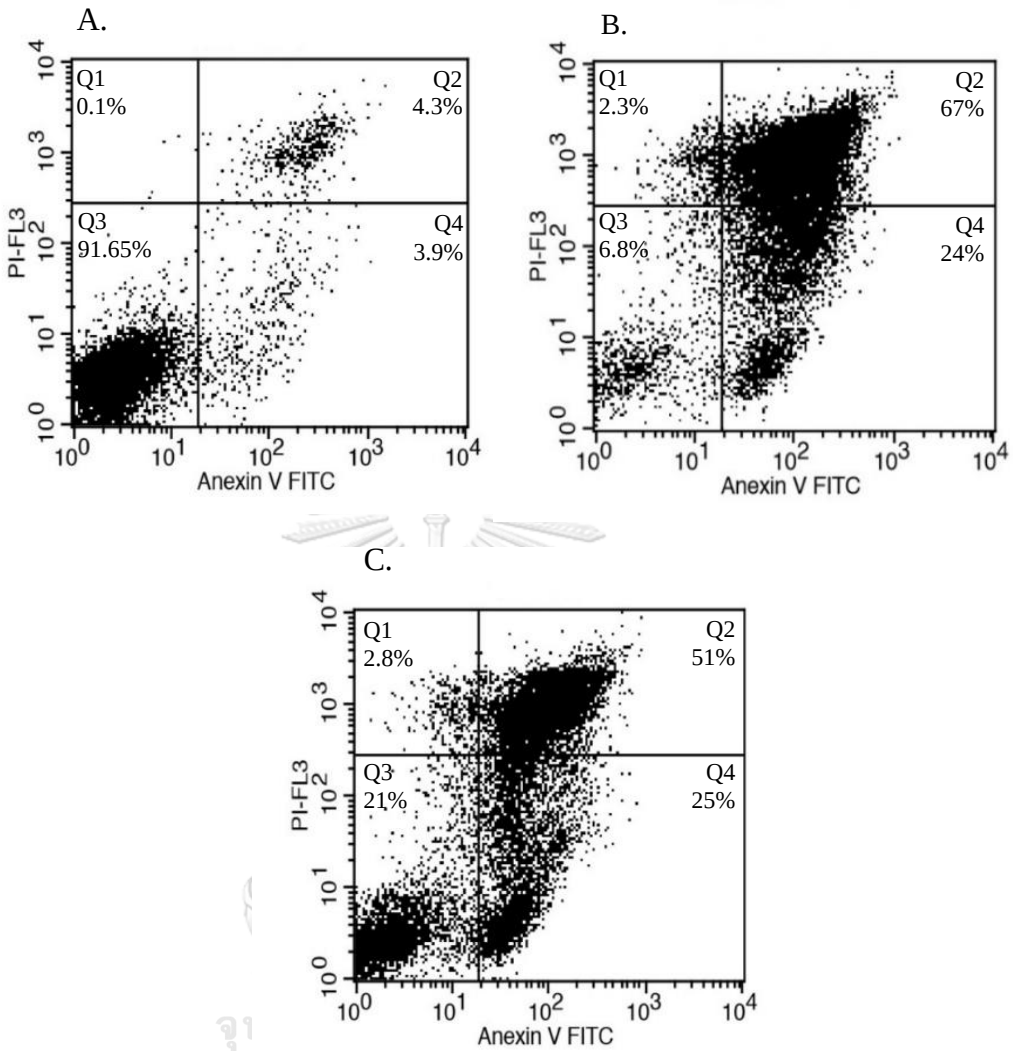

Figure 4. 12 Flow cytometry profile of Jurkat cell. A: untreated cell stained, B: cells treated with 50 µM DAPT (positive control), C: cells treated with 62.5 µM SAHM1-GNPs (20 nm) for 48 h. Quadrant 1 (Q1): necrosis, quadrant 2 (Q2): late apoptosis, quadrant 3 (Q3): live cell, quadrant 4 (Q4): early apoptosis

A

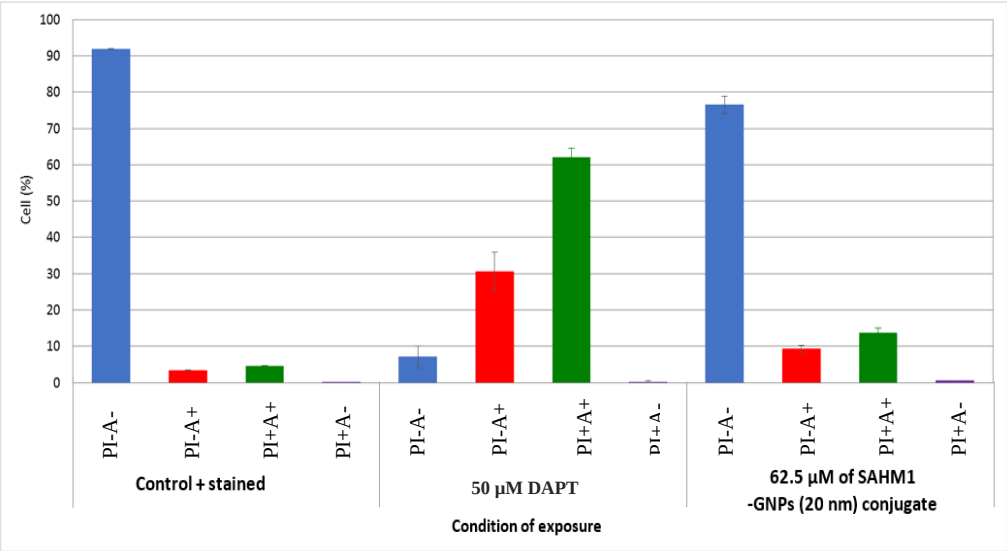

B

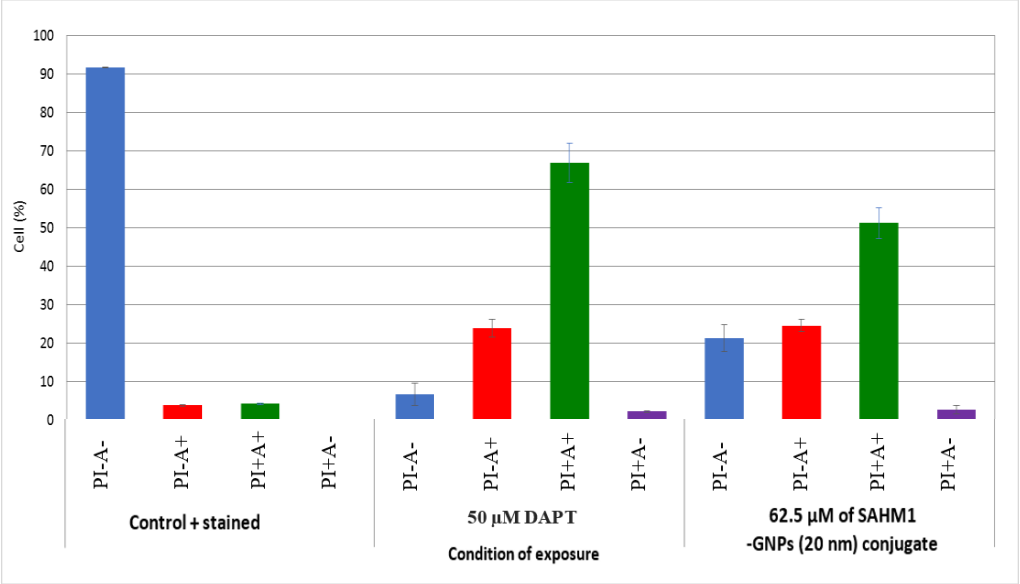

Figure 4. 13 Percentage of Jurkat cells stained with Annexin V and PI after treated with 62.5 µM SAHM1-GNPs (20 nm) or 50 µM DAPT for (A) 24 and (B) 48 h. Where PI-A- : live cells, PI-A+: early apoptotic cells, PI+A+: late apoptotic cells and PI+A- : necrotic cells Data are the mean ± S.D. of three independent experiments of three replicates. Significant differences were analyzed by ANOVA with $P<0.05$.

4.4 Distribution and localization of SAHM1-GNPs

The subcellular localization of GNPs in the Jurkat cells treated with either GNPs or 62.5 µM SAHM1-GNPs (20 nm) at 24 h was determined by TEM as shown in the Figure 4.14. In case of the cell treated with GNPs, GNPs could be found only outside the cell. On the contrary, cell treated with SAHM1-GNPs can be found both outside and inside the cell. It has been reported that SAHM1 was taken up by an active transport mechanism into compartments called endosomes, from which they can reach their target (Moellering et al., 2009). In conclusion, antiproliferative activity and stability of SAHM1 could be enhanced by conjugation on GNP surface via thiolated PEG linker.

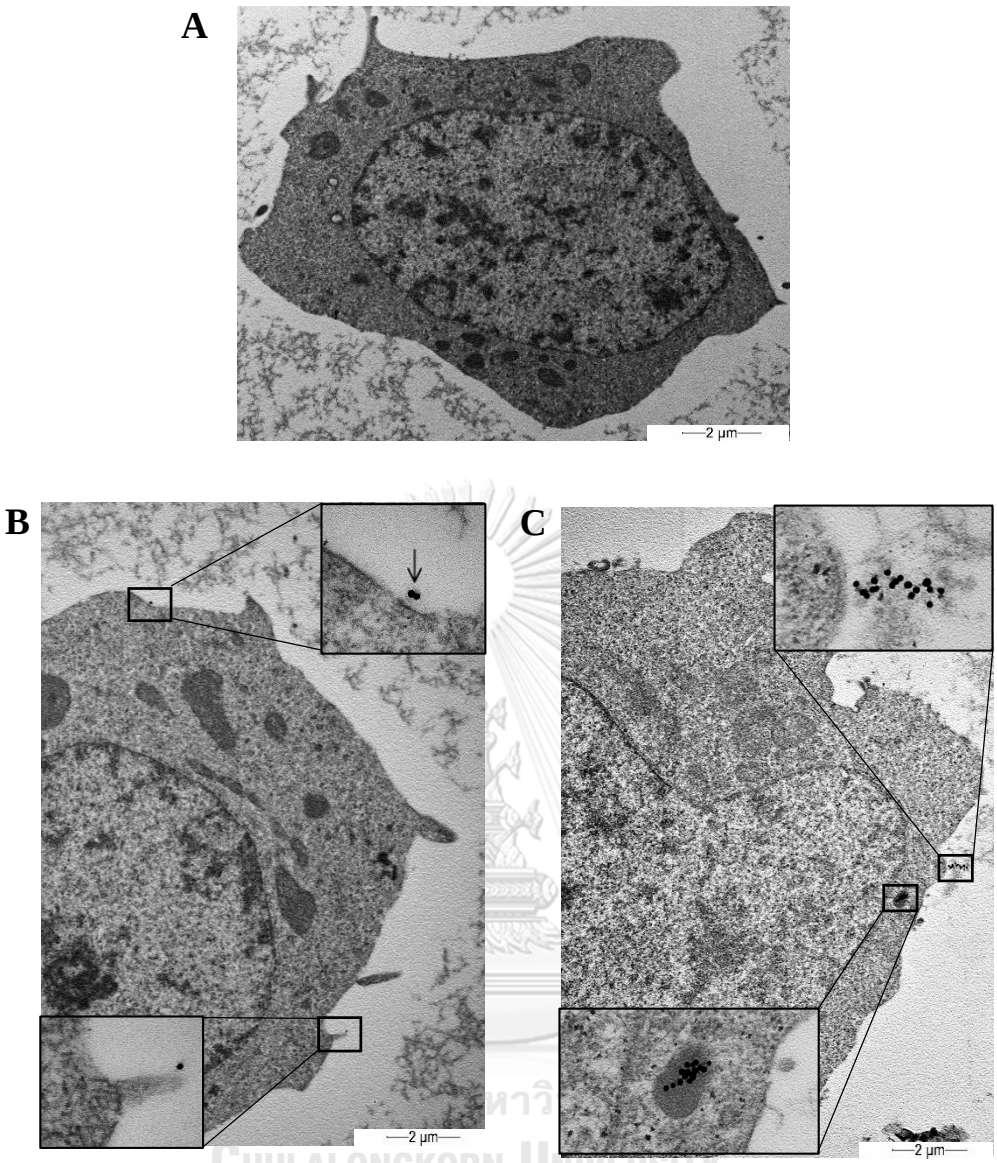

Figure 4. 14 TEM image of subcellular localization of GNPs and SAHM1-GNPs in Jurkat cells. (A) Control cells without GNPs. (B) GNPs (20 nm) treated cells. (C) SAHM1-GNPs (20 nm) treated cells.

From all results, they indicated that GNPs with the size of 20 nm should be used as the carrier for SAHM1 at the low concentration of 62.5 µM. It was expected that the GNPs with small size can express more unique properties such as increased binding affinity and selective targeting to specific tissue or cells than the large size (Tiwari et al., 2014). Moreover, the conjugate showed its antiproliferative activity against Jurkat cell through apoptosis whereas the exact mechanism of antiproliferative activity of SAHM1-GNPs conjugate was still unclear. SAHM1 peptide is one of the therapeutic compounds that have been reported to have anticancer activity (Moellering et al., 2009) that affects NOTCH1 target gene levels and the global expression profile of the NOTCH signaling program in human and murine T-cell acute lymphocytic leukemia (T-ALL). The higher the NOTCH transcription complex production, the higher the risk of cancer recurrence for patients. Thus, GNPs could be used as a carrier of SAHM1 to inhibit the NOTCH transcription and reduce the growth of Jurkat cell.

CHAPTER V

CONCLUSION

Gold nanoparticles (GNPs) were investigated as a carrier for cell penetration to enhance antiproliferative activity of SAHM1 in Jurkat cell line. GNPs were prepared by reduction reaction between trisodium citrate and $HAuCl_4$ at different conditions to obtain the particles with the averaged size of 20 nm, 40 nm and 60nm. Thiolated polyethylene glycol (PEG) was used as the linker for the attachment of SAHM1 onto the GNPs. The amount of SAHM1 used to prepare SAHM1-GNPs was varied to find the optimum concentration which gave the colloidal GNPs or could prevented the aggregation of GNPs. For all sizes of the prepared GNPs, the optimum concentration of SAHM1 was found at 62.5 µM. Cytotoxicity of GNPs, thiolated PEG, thiolated PEG-GNPs, SAHM1 and SAHM1-(thiolated PEG)-GNPs was studied on Jurkat cell line. Cell viabilities of Jurkat cells decreased to about 70% when separately treated with GNPs, SAHM1 and thiolated PEG-GNPs as compared to those of the untreated cells. Cell viabilities of the cell treated with SAHM1-GNPs noticeably decreased only when 20 nm GNPs coated with 62.5 µM and 125 µM SAHM1 were used as compared to those of cells treated with GNPs, thiolated PEG, thiolated PEG-GNPs and SAHM1. Therefore, enhancement of antiproliferative activity of SAHM1 was found when 20 nm GNPs coated with 62.5 µM and 125 µM SAHM1 were used. Cell death after treatment with SAHM1-GNPs for 24 and 48 h was induced by early and late apoptosis stage.

RECOMMENDATION

Enhancement of antiproliferative activity of SAHM1 attached to GNPs via thiolated PEG linker was not significantly improved. It might be due to the reason that only free form of SAHM1 can be recognized by the binding partner and acts as the inhibitor. Therefore, attachment of SAHM1 on the GNPs should be irreversible. After GNPs carry SAHM1 into the cells, SAHM1 must be released inside the cell. Consequently, new linkers should be studied for controllable release of SAHM1 at the target sites.

APPENDIX A

Reagents and Buffers

1. Reagents and buffers for GNP synthesis

1.1 1% by weight $HAuCl_4$

$HAuCl_4 \cdot H_2O$	24.5 g
DDI water	2.45 mL

1.2 1% by weight sodium citrate

Sodium citrate	100 mg
DDI water	10 mL

1.3 10% weight/volume NaCl

NaCl	10 g
DDI water	100 mL

2. Media for Jurkat culture

2.1 RPMI (10% v/v FCS)

Roswell Park Memorial Institute medium (RPMI 1640)	90 mL
Fetal calf serum (FCS)	10 mL

The medium was stored at 4 ^{o}C until use.

2.2 Freezing medium (10% v/v DMSO)

Roswell Park Memorial Institute medium (RPMI 1640)	90 mL
Dimethyl sulfoxide (DMSO)	10 mL

The medium was stored at 4 ^{o}C until use.

3. MTT solution

3.1 5 mg/mL MTT solution

3-(4,5-dimethylthiazol-2-yl)-2,5-diphenyltetrazolium bromide (MTT)	5 mg
DDI water	1 mL

The mixture was stored at 4 ^{o}C until use.

4. Buffer for apoptosis analysis

4.1 20 mM Phosphate buffered saline (PBS) solution, pH 7.2

20 mM KH_2PO_4	2.72 g
20 mM K_2HPO_4	3.48 g
150 mM NaCl	8.77 g
DDI water	1,000 mL

The buffer was adjusted to pH 7.2 and stored at 4 ^{o}C until use.

4.2 20 mM Phosphate buffered saline, pH 7.2 (1% v/v FCS)

20 mM Phosphate buffered saline (PBS) solution	90 mL
Fetal calf serum (FCS)	10 mL

The buffer was stored at 4 ^{o}C until use.

APPENDIX B

Table B. 1 Percentage of Jurkat cell viability after treatment at different conditions for 24 h, 48 h and 72 h

Treatment conditions	Cell viability (%)		
	24 h	48 h	72 h
Untreated cell	100 ± 2.30	100 ± 3.03	100 ± 5.30
DAPT 50 µM	32 ± 1.05	19 ± 1.26	10.3 ± 0.75
20 nm GNPs	82 ± 1.34	80 ± 2.43	88 ± 3.35
40 nm GNPs	79 ± 3.16	89 ± 4.82	88 ± 2.96
60 nm GNPs	83 ± 2.48	91 ± 2.30	93 ± 3.12
62.5 µM thiolated PEG	82.7 ± 0.56	88 ± 1.64	80 ± 2.24
125 µM thiolated PEG	76 ± 2.66	77 ± 1.98	81 ± 2.55
250 µM thiolated PEG	75 ± 2.87	75 ± 2.36	80 ± 1.63
62.5 µM SAHM1	81 ± 3.45	83 ± 2.49	88 ± 4.65
125 µM SAHM1	74 ± 2.91	69 ± 2.13	79 ± 3.53
250 µM SAHM1	66 ± 2.73	70 ± 3.56	78 ± 4.63
62.5 µM thiolated PEG - GNPs (20 nm)	83 ± 3.62	95 ± 2.09	102 ± 3.21
125 µM thiolated PEG - GNPs (20 nm)	85 ± 2.53	80 ± 3.51	83 ± 4.01
250 µM thiolated PEG - GNPs (20 nm)	65 ± 2.49	73 ± 1.67	75 ± 3.93
62.5 µM thiolated PEG - GNPs (40 nm)	58 ± 2.68	62 ± 3.93	71 ± 4.01
125 µM thiolated PEG - GNPs (40 nm)	60 ± 2.00	61.1 ± 0.88	72 ± 3.63
250 µM thiolated PEG - GNPs (40 nm)	74 ± 4.57	87 ± 3.02	88 ± 3.60
62.5 µM thiolated PEG - GNPs (60 nm)	58 ± 3.47	63 ± 2.98	69 ± 1.84
125 µM thiolated PEG - GNPs (60 nm)	56 ± 1.50	63.9 ± 0.99	68 ± 3.52
250 µM thiolated PEG - GNPs (60 nm)	60 ± 2.50	70 ± 3.89	81 ± 2.02
62.5 µM SAHM1- GNPs (20 nm)	56 ± 1.93	50 ± 1.70	59 ± 2.31
125 µM SAHM1- GNPs (20 nm)	48 ± 2.89	66 ± 1.14	63 ± 4.28
250 µM SAHM1- GNPs (20 nm)	51.8 ± 0.63	66 ± 2.84	67 ± 3.27
62.5 µM SAHM1- GNPs (40 nm)	80 ± 1.63	69 ± 3.01	87 ± 2.35
125 µM SAHM1- GNPs (40 nm)	77 ± 2.47	82 ± 3.42	82 ± 1.93
250 µM SAHM1- GNPs (40 nm)	63 ± 3.86	69 ± 1.06	67 ± 3.75
62.5 µM SAHM1- GNPs (60 nm)	67 ± 2.35	78 ± 4.03	76 ± 3.10
125 µM SAHM1- GNPs (60 nm)	55 ± 4.92	69 ± 3.20	74 ± 4.87
250 µM SAHM1- GNPs (60 nm)	67 ± 1.28	66 ± 3.01	72 ± 4.65

(Data are the mean±SD of three independent experiments of three replicates.)

Table B. 2 Percentage of Jurkat cells stained with Annexin V and PI after treated with 62.5 µM SAHM1-GNPs (20 nm) or 50 µM DAPT for 24 h

	Percentage of Jurkat cells at 24 h			
	Live	**Early apoptosis**	**Late apoptosis**	**Necrosis**
Control stained	91.9 ± 0.10	3.4 ± 0.14	4.67 ± 0.04	0.02 ± 0.00
50 µM DAPT	7.1 ± 2.94	31 ± 5.30	62 ± 2.54	0.26 ± 0.21
62.5 µM SAHM1-GNPs (20 nm)	76 ± 2.35	9.3 ± 0.98	14 ±1.40	0.54 ± 0.03

(Data are the mean±SD of three independent experiments of three replicates.)

Table B. 3 Percentage of Jurkat cells stained with Annexin V and PI after treated with 62.5 µM SAHM1-GNPs (20 nm) or 50 µM DAPT for 48 h

	Percentage of Jurkat cells at 48 h			
	Live	**Early apoptosis**	**Late apoptosis**	**Necrosis**
Control stained	91.65 ± 0.06	3.9 ± 0.17	4.3 ± 0.17	0.10 ± 0.06
50 µM DAPT	6.8 ± 2.98	24 ± 2.28	67 ± 5.06	2.3 ± 0.20
62.5 µM SAHM1-GNPs (20 nm)	21 ± 3.54	25 ± 1.58	51 ± 4.07	2.8 ± .05

(Data are the mean±SD of three independent experiments of three replicates.)

REFERENCES

Akrami, M., Balalaie, S., Hosseinkhani, S., Alipour, M., Salehi, F., Bahador, A.*, et al.* (2016). Tuning the anticancer activity of a novel pro-apoptotic peptide using gold nanoparticle platforms. *Scientific reports, 6*, 31030.

Anker, J. N., Hall, W. P., Lyandres, O., Shah, N. C., Zhao, J., and Van Duyne, R. P. (2008). Biosensing with plasmonic nanosensors. *Nature materials, 7*(6), 442.

Bantz, C., Koshkina, O., Lang, T., Galla, H.-J., Kirkpatrick, C. J., Stauber, R. H.*, et al.* (2014). The surface properties of nanoparticles determine the agglomeration state and the size of the particles under physiological conditions. *Beilstein journal of nanotechnology, 5*, 1774.

Cai, W., Gao, T., Hong, H., and Sun, J. (2008). Applications of gold nanoparticles in cancer nanotechnology. *Nanotechnology, science and applications, 1*, 17.

Chanda, N., Kattumuri, V., Shukla, R., Zambre, A., Katti, K., Upendran, A.*, et al.* (2010). Bombesin functionalized gold nanoparticles show in vitro and in vivo cancer receptor specificity. *Proceedings of the National Academy of Sciences, 107*(19), 8760-8765.

Chithrani, B. D., Ghazani, A. A., and Chan, W. C. (2006). Determining the size and shape dependence of gold nanoparticle uptake into mammalian cells. *Nano letters, 6*(4), 662-668.

Clogston, J. D., and Patri, A. K. (2011). Zeta potential measurement *Characterization of nanoparticles intended for drug delivery* (pp. 63-70): Springer.

Elmore, S. (2007). Apoptosis: a review of programmed cell death. *Toxicologic pathology, 35*(4), 495-516.

Giljohann, D. A., Seferos, D. S., Daniel, W. L., Massich, M. D., Patel, P. C., and Mirkin, C. A. (2010). Gold nanoparticles for biology and medicine. *Angewandte Chemie International Edition, 49*(19), 3280-3294.

Guo, Q., Guo, Q., Yuan, J., and Zeng, J. (2014). Biosynthesis of gold nanoparticles using a kind of flavonol: Dihydromyricetin. *Colloids and Surfaces A: Physicochemical and Engineering Aspects, 441*, 127-132.

Haiss, W., Thanh, N. T., Aveyard, J., and Fernig, D. G. (2007). Determination of size and concentration of gold nanoparticles from UV− Vis spectra. *Analytical chemistry, 79*(11), 4215-4221.

Jain, P. K., Lee, K. S., El-Sayed, I. H., and El-Sayed, M. A. (2006). Calculated absorption and scattering properties of gold nanoparticles of different size, shape, and composition: applications in biological imaging and biomedicine. *The journal of physical chemistry B, 110*(14), 7238-7248.

Juvé, V., Cardinal, M. F., Lombardi, A., Crut, A., Maioli, P., Pérez-Juste, J.*, et al.* (2013). Size-dependent surface plasmon resonance broadening in nonspherical nanoparticles: single gold nanorods. *Nano letters, 13*(5), 2234-2240.

Kalmodia, S., Vandhana, S., Rama, B. T., Jayashree, B., Seethalakshmi, T. S., Umashankar, V.*, et al.* (2016). Bio-conjugation of antioxidant peptide on surface-modified gold nanoparticles: a novel approach to enhance the radical scavenging property in cancer cell. *Cancer nanotechnology, 7*(1), 1.

Khan, A., Rashid, R., Murtaza, G., and Zahra, A. (2014). Gold nanoparticles: synthesis and applications in drug delivery. *Tropical Journal of Pharmaceutical Research, 13*(7), 1169-1177.

Khlebtsov, N. G. (2008). Determination of size and concentration of gold nanoparticles from extinction spectra. *Analytical chemistry, 80*(17), 6620-6625.

Kim, C. K., Ghosh, P., Pagliuca, C., Zhu, Z.-J., Menichetti, S., and Rotello, V. M. (2009). Entrapment of hydrophobic drugs in nanoparticle monolayers with efficient release into cancer cells. *Journal of the American Chemical Society, 131*(4), 1360-1361.

Kojima, C., Umeda, Y., Harada, A., and Kono, K. (2010). Preparation of near-infrared light absorbing gold nanoparticles using polyethylene glycol-attached dendrimers. *Colloids and Surfaces B: Biointerfaces, 81*(2), 648-651.

Kumar, D., Meenan, B. J., Mutreja, I., D'SA, R., and Dixon, D. (2012). Controlling the size and size distribution of gold nanoparticles: a design of experiment study. *International Journal of Nanoscience, 11*(02), 1250023.

Kurosaka, K., Takahashi, M., Watanabe, N., and Kobayashi, Y. (2003). Silent cleanup of very early apoptotic cells by macrophages. *The Journal of Immunology, 171*(9), 4672-4679.

Lee, D., Ko, W.-K., Hwang, D.-S., Heo, D. N., Lee, S. J., Heo, M.*, et al.* (2016). Use of baicalin-conjugated gold nanoparticles for apoptotic induction of breast cancer cells. *Nanoscale research letters, 11*(1), 381.

Manohar, S., Rayavarapu, R., Petersen, W., and van Leeuwen, T. G. (2009). *Cell viability studies of PEG-thiol treated gold nanorods as optoacoustic contrast agents.* Paper presented at the Photons Plus Ultrasound: Imaging and Sensing 2009.

Marino, B. S., and Fine, K. S. (2013). *Blueprints pediatrics* (Vol. 6): Lippincott Williams & Wilkins.

Mody, V. V., Siwale, R., Singh, A., and Mody, H. R. (2010). Introduction to metallic nanoparticles. *Journal of Pharmacy and Bioallied Sciences, 2*(4), 282.

Moellering, R. E., Cornejo, M., Davis, T. N., Del Bianco, C., Aster, J. C., Blacklow, S. C.*, et al.* (2009). Direct inhibition of the NOTCH transcription factor complex. *Nature, 462*(7270), 182.

Nativo, P., Prior, I. A., and Brust, M. (2008). Uptake and intracellular fate of surface-modified gold nanoparticles. *ACS nano, 2*(8), 1639-1644.

Nefedova, Y., Sullivan, D. M., Bolick, S. C., Dalton, W. S., and Gabrilovich, D. I. (2008). Inhibition of Notch signaling induces apoptosis of myeloma cells and enhances sensitivity to chemotherapy. *Blood, 111*(4), 2220-2229.

Norbury, C. J., and Hickson, I. D. (2001). Cellular responses to DNA damage. *Annual review of pharmacology and toxicology, 41*(1), 367-401.

Pan, Y., Neuss, S., Leifert, A., Fischler, M., Wen, F., Simon, U.*, et al.* (2007). Size-dependent cytotoxicity of gold nanoparticles. *Small, 3*(11), 1941-1949.

Qian, W., Curry, T., Che, Y., and Kopelman, R. (2013). *Targeted delivery of peptide-conjugated biocompatible gold nanoparticles into cancer cell nucleus.* Paper presented at the Colloidal Nanocrystals for Biomedical Applications VIII.

Rathinaraj, P., and Al-Jumaily, A. M. (2015). internalization: acute apoptosis of breast cancer cells using herceptin-immobilized gold nanoparticles. *Breast Cancer: Targets and Therapy, 7*, 51.

Riccio, O., Van Gijn, M. E., Bezdek, A. C., Pellegrinet, L., Van Es, J. H., Zimber-Strobl, U.*, et al.* (2008). Loss of intestinal crypt progenitor cells owing to inactivation of both Notch1 and Notch2 is accompanied by derepression of CDK inhibitors p27Kip1 and p57Kip2. *EMBO reports, 9*(4), 377-383.

Rice, S. B., Chan, C., Brown, S. C., Eschbach, P., Han, L., Ensor, D. S.*, et al.* (2013). Particle size distributions by transmission electron microscopy: an interlaboratory comparison case study. *Metrologia, 50*(6), 663.

Rock, K. L., and Kono, H. (2008). The inflammatory response to cell death. *Annu. Rev. pathmechdis. Mech. Dis., 3*, 99-126.

Savill, J., and Fadok, V. (2000). Corpse clearance defines the meaning of cell death. *Nature, 407*(6805), 784.

Shim, E. J., Hahm, B. J., Yu, E. S., Kim, H. K., Cho, S. J., Chang, S. M.*, et al.* (2017). Development and validation of the National Cancer Center Psychological Symptom Inventory. *Psycho-oncology, 26*(7), 1036-1043.

Smith, M., Arthur, D., Camitta, B., Carroll, A. J., Crist, W., Gaynon, P.*, et al.* (1996). Uniform approach to risk classification and treatment assignment for children with acute lymphoblastic leukemia. *Journal of Clinical Oncology, 14*(1), 18-24.

Tiwari, P. M., Eroglu, E., Bawage, S. S., Vig, K., Miller, M. E., Pillai, S.*, et al.* (2014). Enhanced intracellular translocation and biodistribution of gold nanoparticles functionalized with a cell-penetrating peptide (VG-21) from vesicular stomatitis virus. *Biomaterials, 35*(35), 9484-9494.

Tkachenko, A., Xie, H., Franzen, S., and Feldheim, D. L. (2005). Assembly and characterization of biomolecule-gold nanoparticle conjugates and their use in intracellular imaging *Nanobiotechnology protocols* (pp. 85-99): Springer.

Tripathi, V., Nara, S., Singh, K., Singh, H., and Shrivastav, T. G. (2012). A competitive immunochromatographic strip assay for 17-α-hydroxy progesterone using colloidal gold nanoparticles. *Clinica Chimica Acta, 413*(1-2), 262-268.

Turkevich, J., Stevenson, P. C., and Hillier, J. (1951). A study of the nucleation and growth processes in the synthesis of colloidal gold. *Discussions of the Faraday Society, 11*, 55-75.

Wei, X.-L., Mo, Z.-H., Li, B., and Wei, J.-M. (2007). Disruption of HepG2 cell adhesion by gold nanoparticle and Paclitaxel disclosed by in situ QCM measurement. *Colloids and Surfaces B: Biointerfaces, 59*(1), 100-104.

Yang, C., Bromma, K., and Chithrani, D. (2018). Peptide mediated in vivo tumor targeting of nanoparticles through optimization in single and multilayer in vitro cell models. *Cancers, 10*(3), 84.

Zhang, C., Yang, Y., Zhou, X., Liu, X., Song, H., He, Y.*, et al.* (2010). Highly pathogenic avian influenza A virus H5N1 NS1 protein induces caspase-dependent apoptosis in human alveolar basal epithelial cells. *Virology Journal, 7*(1), 51.

Zhang, X. (2015). Gold nanoparticles: recent advances in the biomedical applications. *Cell biochemistry and biophysics, 72*(3), 771-775.

VITA

Miss Mukthida Thippayamonta was born on 2nd January 1992 in Phatthalung, Thailand. She graduated with Bachelor Degree of Science from Department of Biotechnology, Faculty of Science, Mahidol University in 2014. She decided to study for her Master Degree of Science in Biotechnology, Faculty of Science, Chulalongkorn University in 2015.

Academic presentations;

1. Mukthida Thippayamonta, Songchan Puthong, Stephan T. Dubas, Tanapat Palaga and Kittinan Komolpis. ANTIPROLIFERATIVE ACTIVITY OF GOLD NANOPARTICLE-SAHM1 PEPTIDE CONJUGATE AGAINST JURKAT CELLS. 29th Annual Meeting of Thai Society for Biotechnology and International Conference (TSB 2017), November 23-25, 2017, Swissotel Le Concorde, Bangkok, Thailand